

On the regional-scale variability of flow duration curves in Peninsular India

Pankaj Dey¹, Jeenu Mathai², Murugesu Sivapalan^{3,4} and Pradeep. P. Mujumdar^{5,6}

¹Department of Hydrology, Indian Institute of Technology, Roorkee, India

²Marine Geoscience Group, National Centre for Earth Science Studies, Thiruvananthapuram, India

³Department of Civil and Environmental Engineering, University of Illinois at Urbana-Champaign, Urbana, IL, USA

⁴Department of Geography and Geographic Information Science, University of Illinois at Urbana-Champaign, Urbana, IL, USA

⁵Department of Civil Engineering, Indian Institute of Science, Bangalore, India

⁶Interdisciplinary Centre for Water Research, Indian Institute of Science, Bangalore, India

Correspondence to: Pankaj Dey (pdey609@gmail.com)

Abstract. Peninsular India is a unique region with major mountain ranges which govern regional atmospheric circulation and precipitation variability, the monsoons and regional geology at range of time and process scales. The controls of landscape and climatic features on streamflow variability at a regional scale using flow duration curve (FDC) – a compact description of streamflow variability, offering a window into the multiple, interacting processes that contribute to streamflow variability – is less explored. This study explores the suitability of partitioning of annual streamflow FDC into seasonal FDCs, and total streamflow FDC into fast and slow flow FDCs to unravel the process controls on FDCs at a regional scale, with application to low-gradient rivers flowing east from the Western Ghats of Peninsular India. The results indicate that bimodal rainfall seasonality and subsurface gradients explain the higher contribution of slow flow to total flow across north-south gradient of the region. Shapes of fast and slow FDCs are controlled by recession parameters revealing the role of climate seasonality and geologic profiles, respectively. A systematic spatial variation across north-south gradient is observed– highlighting the importance of coherent functioning of landscape-hydroclimate settings in imparting distinct signature of streamflow variability. The framework is useful to discover the role of time and process controls on streamflow variability in a region with seasonal hydro-climatology and hydro-geologic gradients.

1 Introduction

The hydrologic functioning of catchment systems in any given region is coevolved with the long-term climatology and landscape features present in the region through mutual interactions operating across multiple spatial and temporal scales (Wagener et al., 2013). These interactions and long-term feedbacks impart variability to hydrologic processes that are characteristic of the region of interest, including runoff generation and riverine transport processes, thus influencing water availability and reliability to human populations that depend on the streamflow. Understanding streamflow variability in time and space across river basins in the region is therefore very important for water resource management (Deshpande et al., 2016; Sinha et al., 2018) and the prediction and

37 mitigation of floods (Kale et al., 1997). The frequency of high flows, low flows, or flows within specific ranges,
38 is essential for risk assessment of water management projects involving control of streamflow variability. Correct
39 portrayal of streamflow variability at the scale of catchments and river basins is therefore an indispensable
40 component in many hydrologic applications.

41 The focus of this paper is on the flow duration curve (FDC), which is a compact description of temporal
42 streamflow variability at the catchment scale. The FDC represents (daily) streamflow values plotted against the
43 proportion of time the given flow is exceeded or equalled (Smakhtin, 2001; Vogel & Fennessey, 1994). The
44 graphical form of the FDC embeds the governing hydrologic processes and dominant flow characteristics
45 throughout the range of recorded streamflow at the catchment scale (Botter et al., 2008). In this sense, the FDC is
46 also an important signature of a catchment's rainfall to runoff transformation (Ghotbi et al., 2020a; Vogel &
47 Fennessey, 1994). FDC thus typifies the old proverb, "one picture is worth a thousand words" with its potential
48 to encapsulate much of the relevant information of streamflow variability in a single plot (Vogel & Fennessey,
49 1995), and has been used in many hydrologic applications. Vogel and Fennessey (1994) provide a brief history of
50 the application of flow duration curves in hydrology. Applications of FDC include waste load allocation (Searcy,
51 1959), water quality management (Searcy, 1959; Rehana & Mujumdar, 2011, 2012), reservoir and sedimentation
52 studies (Vogel & Fennessey, 1995), low-flow and flood analyses (Smakhtin, 2001), assessment of environmental
53 flow requirements (Smakhtin and Anputhas, 2006), and water availability for hydropower (Basso & Botter, 2012).

54 Streamflow observed in rivers results from the complex interplay of various hydrological processes, including
55 runoff generation, overland and subsurface flow, and evaporation. These processes operate across multiple time
56 and space scales, responding to climatic inputs and interacting with heterogeneous landscape properties.
57 Deciphering the controls on streamflow variability and understanding their manifestation in the FDC shape pose
58 significant challenges (Cheng et al., 2012; Ghotbi et al., 2020b; Yokoo & Sivapalan, 2011). Therefore, identifying
59 the process controls is essential to develop appropriate conceptual frameworks. This approach enables the
60 generation of profound insights into the governing principles that underpin the observed variability in catchments.

61 To address this complexity, Yokoo and Sivapalan (2011) proposed a conceptual framework for unravelling the
62 process controls of the FDC. They considered the Total Flow Duration Curve (TFDC) as a statistical summation
63 of a Fast Flow Duration Curve (FFDC) and a Slow Flow Duration Curve (SFDC). The FFDC, representing a
64 filtered version of precipitation variability, is influenced by rainfall intensity patterns and surface soil
65 characteristics. In contrast, the SFDC reflects the competition between subsurface drainage and
66 evapotranspiration, with seasonality and regional geology playing stronger roles (Yokoo & Sivapalan, 2011). This
67 distinction between fast (surface runoff) and slow (subsurface streamflow and groundwater flow) flow time scales
68 allows for a nuanced understanding of the process controls governing each component separately (Cheng et al.,
69 2012; Yokoo & Sivapalan, 2011).

70 Ghotbi et al (2020a, 2020b) used this framework to explore the climatic and landscape controls of FDCs using
71 streamflow data for hundreds of catchments across the continental United States in a comparative manner. In
72 their work Ghotbi et al. (2020a) emphasized the need to consider the fast flow and slow flow time series
73 independently as stochastic responses of catchments to sequences of storm events. Intensity and frequency of
74 rainfall events and the properties of soils and topography govern the variability of fast flows, whereas climate

75 seasonality and regional geology of the aquifer system govern variability of slow flow components. More
76 specifically, Ghotbi et al. (2020b) showed the dominant process controls of FDCs as aridity index, topographic
77 slope, coefficient of variation of daily precipitation, timing of rainfall, time interval between storms, snow fraction,
78 and recession slope.

79 Stewart (2015) introduces the Bump and Rise Method (BRM), a novel baseflow separation technique calibrated
80 with tracer data or optimization methods for accurate replication of tracer-determined baseflow shapes. The study
81 challenges the conventional practice of solely relying on streamflow for recession analysis, contending that it can
82 be misleading in understanding catchment storage reservoirs. The study also suggests for implementing baseflow
83 separation before recession analysis as a means to gain fresh insights into water storage reservoirs and potentially
84 resolve existing issues associated with recession analysis.

85 Significant advancements have been achieved in unravelling the process controls influencing flow duration
86 curves. However, challenges persist in extending this knowledge to large spatial scales. To address this, Leong
87 and Yokoo (2022) proposed an innovative approach, aiming to enhance the flexibility and adaptability of
88 hydrological models by transforming the representation of the subsurface component. This involves the creation
89 of a flexible structure composed of interconnected linear reservoirs, derived from a distinctive multiple
90 hydrograph separation procedure, offering a comprehensive interpretation of dominant processes impacting FDC
91 shapes and understand the number of distinct hydrological processes involved. In this study, we adopted the
92 method proposed by Ghotbi et al. (2020) and (2021) as a foundational step to characterize fast and slow flow
93 components, recognizing its inherent limitations stemming from its empirical and subjective nature.

94 Botter et al. (2008) addressed river basin streamflow variability by presenting a seasonal probability distribution
95 for daily streamflow using a stochastic soil moisture model. Extending this to the annual scale, the study
96 establishes analytical expressions for long-term flow duration curves, linking them to annual minima distribution
97 through key basin parameters, including climate, ecohydrology, and geomorphology. Muller et al. (2014) presents
98 a process-based analytical expression for flow duration curves in seasonally dry climates, employing a stochastic
99 model for wet season streamflow and a deterministic recession with stochastic initial conditions for the dry season.
100 The approach disentangles inter- and intra-annual streamflow variations effectively. Durighetto et al. (2022)
101 develops analytical expressions for flow duration curves and stream length duration curves (SLDC) to classify
102 streamflow and active length regimes in temporary rivers. It identifies two streamflow regimes (persistent and
103 erratic) and three active length regimes (ephemeral, perennial, and ephemeral de facto) based on dimensionless
104 parameters linked to streamflow fluctuations and catchment discharge sensitivity. The proposed framework,
105 validated in Italy and USA catchments, reveals a structural relationship between streamflow and active length
106 regimes, offering a promising tool for analysing discharge and river network length dynamics in temporary
107 streams.

108 Our approach to understanding spatial patterns across Peninsular India builds upon the foundational concept of
109 timescale decomposition, as previously explored in studies such as Botter et al. (2008), Muller et al. (2014), and
110 Durighetto et al. (2022). The decomposition of timescales, while not novel in our study, serves as a fundamental
111 framework, aiding our analysis of spatial dynamics in the region.

112 Leong and Yokoo (2022) introduced an innovative approach, employing interconnected linear reservoirs to
113 enhance hydrological model flexibility and adaptability. Carlier et al. (2018) addressed the neglect of geological
114 characteristics in catchment studies, revealing that climate conditions predominantly influence medium to high
115 discharge percentiles, while the catchment's ability to buffer meteorological forcing is attributed to geological
116 features. Botter et al. (2013) identified an index incorporating climate and landscape attributes to discriminate
117 between erratic and persistent flow regimes, providing a robust framework for characterizing hydrology in the
118 face of global change. Basso et al. (2015) investigated the role of non-linear storage–discharge relations in shaping
119 high-flow distributions, emphasizing the importance of analysing individual events for accurate characterization.
120 Ye et al. (2012) explored regional variations in streamflow regime behaviour across the U.S., highlighting the
121 significance of snowmelt, vegetation cover dynamics, and climate trends. Fenicia et al. (2014) linked perceptual
122 hydrological models with mathematical structures, demonstrating how distinct catchment processes influence
123 model performance and emphasizing the need to synthesize experimentalist and modeler perspectives. Together,
124 these studies contribute to a comprehensive understanding of FDCs and advance our knowledge of hydrological
125 processes at different scales.

126 While the existing literature, represented by studies such as Leong and Yokoo (2022), Carlier et al. (2018), Botter
127 et al. (2013), Basso et al. (2015), Ye et al. (2012), and Fenicia et al. (2014), has made significant strides in
128 understanding the controls of flow duration curves and streamflow variability, our study distinguishes itself by
129 focusing on the unique hydrological context of Peninsular India. The previously discussed works have primarily
130 addressed FDC drivers at regional or global scales, examining factors such as hydrogeology, climate, and
131 landscape alterations. In contrast, our study delves into the specific challenges posed by the Peninsular Indian
132 environment, characterized by the interplay of monsoons, mountainous terrain, and topographical gradients.
133 Through a comprehensive approach encompassing time scale decomposition and process decomposition, and
134 statistical analyses, we employ FDC as a key tool to unravel the controls of streamflow variability across
135 Peninsular India. Our work enhances the understanding of hydrological processes in a region with distinct
136 monsoonal influences, thus advancing the state of the art and providing valuable insights for water resource
137 management in Peninsular India.

138 The novelty of the paper lies in exploring the controls of streamflow variability in Peninsular India, a result of the
139 impacts of monsoons – southwest (summer season) and northeast (winter season) – the presence of western and
140 eastern ghats, and topographical gradients. The paper advances the field by partitioning streamflow into three
141 distinct time-wise categories (non-monsoon, southwest monsoon, and northeast monsoon) and two process-wise
142 partitions (fast flow and slow flow), using flow duration curves as a tool. This approach allows for a detailed
143 examination of the relative contributions of each season and process to the overall annual flow. Furthermore, the
144 integration of a comprehensive approach to analysing flow duration curves by incorporating a Mixed Gamma
145 Distribution (MGD) to model both fast and slow flow components, along with seasonal and regional exploration,
146 enhances the study's novelty. The study uncovers the influence of climate, geology, and hydrological processes
147 on MGD parameters, providing a better understanding of flow duration curve shapes. The inclusion of links
148 between MGD parameters and landscape properties, as well as the association between the midsection slope of
149 the FDC and recession parameters, adds an additional layer of sophistication to the analysis. We recognize the
150 abundance of literature in FDC studies, but we believe our contribution is distinctive due to its innovative

151 combination of partitioning techniques and statistical analysis, offering deeper insights into spatial variations and
152 emphasizing the intertwined influence of surface and subsurface processes on streamflow patterns in the region.

153 The remainder of the paper is structured as follows. Section 2 elaborates on the details of the study area and the
154 daily streamflow dataset used. The description of the methodology employed for the analysis is presented in
155 Section 3. The results of the application of the framework to Peninsular India and the interpretation of the results
156 are presented in Sections 4 and 5, respectively. Finally, the paper is concluded in Section 6 with key insights
157 gained for the nature and controls of streamflow variability across Peninsular India.

158 **2 Study region**

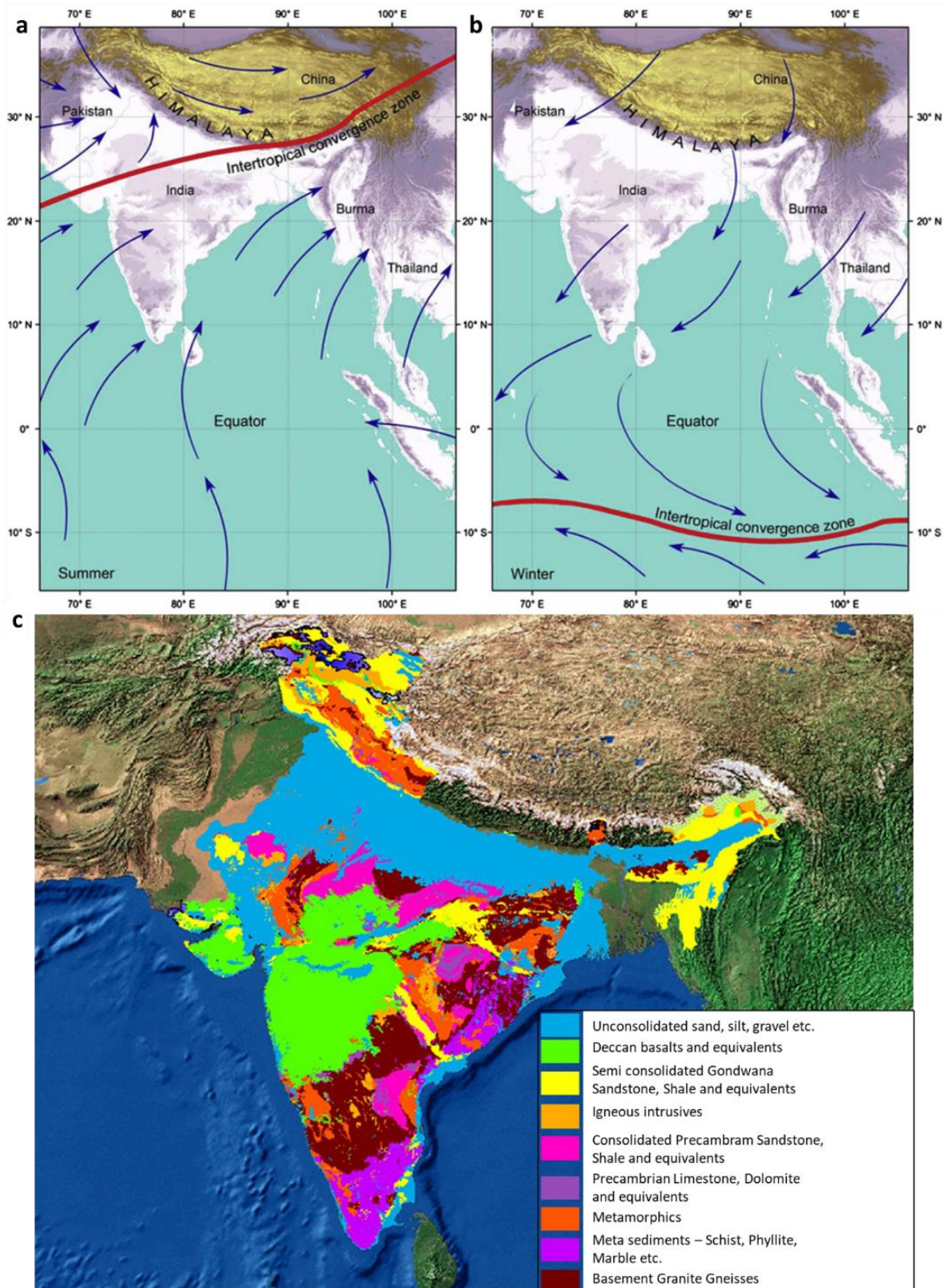
159 Peninsular India is a cratonic region with an approximate shape of a vast inverted triangle with diverse topography
160 and characteristic climatic patterns, bounded by the Arabian Sea in the west, the Bay of Bengal in the east, and
161 the Vindhya and Satpura ranges in the north. The long escarpments of the Western Ghats and the Eastern Ghats,
162 constituting the western and eastern continental fringes of India, and an asymmetric relief with eastward tilt
163 towards the floodplains of several eastward draining rivers from the 1.5 km high Western Ghats, characterize the
164 physiography of Peninsular India (Richards et al., 2016). The rise of the Himalayan-Tibetan plateau has
165 significantly contributed to the Neogene climate of Asia, favoured the birth of the modern monsoon (Fig. 1.a, b)
166 (Chatterjee et al., 2013, 2017), and triggered glaciation in the Northern region. A wide variety of plateaux, open
167 valleys, bedrock gorges, mountain ranges, inselbergs and residual hills constitute the geomorphology of
168 Peninsular India (Kale & Vaidyanadhan, 2014). The Peninsular landscape is dominated by Deccan Traps (Deccan
169 basalts) of Cretaceous-Eocene, igneous and metamorphic rocks (Granite-gneisses) of Archaean-Late Precambrian
170 along with minor consolidated sediments (Sandstone, shale) of Precambrian-Jurassic (Fig. 1.c) (Kale, 2014).

171 The region is strongly impacted by monsoons, major seasonal winds which are a manifestation of the seasonal
172 movement of the Intertropical Convergence Zone (ICTZ in Fig. 1.a and Fig. 1.b), which contribute largely to the
173 annual rainfall variability in much of the Indian subcontinent (Gadgil, 2003). The monsoons have two components
174 – South-West monsoon and North-East monsoon, which arrive during June – September (JJAS) and October –
175 December (OND), respectively. South-West monsoon season contributes more than 75% of annual rainfall over
176 majority of the regions of the country (Saha et al., 1979). However, the Southern Peninsula receives a significant
177 portion (30-60%) of its annual rainfall during the North-East monsoon, which contributes only 11% of the rainfall
178 annually to India as a whole (Rajeevan et al., 2012). The maximum extent of rainfall over the Southern Peninsula
179 during the North-East Monsoon is due to the reversal of lower-level winds over South Asia from the South-West
180 to the North-East during the retreating phase of the South-West monsoon (Rajeevan et al., 2012). Peninsular India
181 displays south-to-north variability in the South-West monsoon, causing heavy rainfall along the Western Ghats
182 and reduced amounts in the central and northeastern regions (Fig S2.a in Supplementary Material).

183 The Western Ghats' long escarpment hosts predominantly tropical evergreen forest, crucial for intercepting South-
184 West monsoon winds (Ramachandra, 2018). Ramachandra (2018) depicted a west-east vegetation gradient along
185 the Western Ghats, transitioning from tropical-evergreen to semi-evergreen and progressing to moist to dry
186 deciduous forests towards the rain-shadow region in the east. The topography map for the Peninsular region and
187 a selected point in the region is depicted in Fig. S1.a and Fig. S1.b in Supplementary Material, respectively. The
188 western margin of Peninsular India, influenced by the Western Ghats, receives heavy rainfall, while the rain

189 shadow region experiences deficient rainfall (Fig. S2.c). The geological and tectonic history, coupled with
190 monsoon climate events, has significantly shaped the present landform (Kale, 2014).

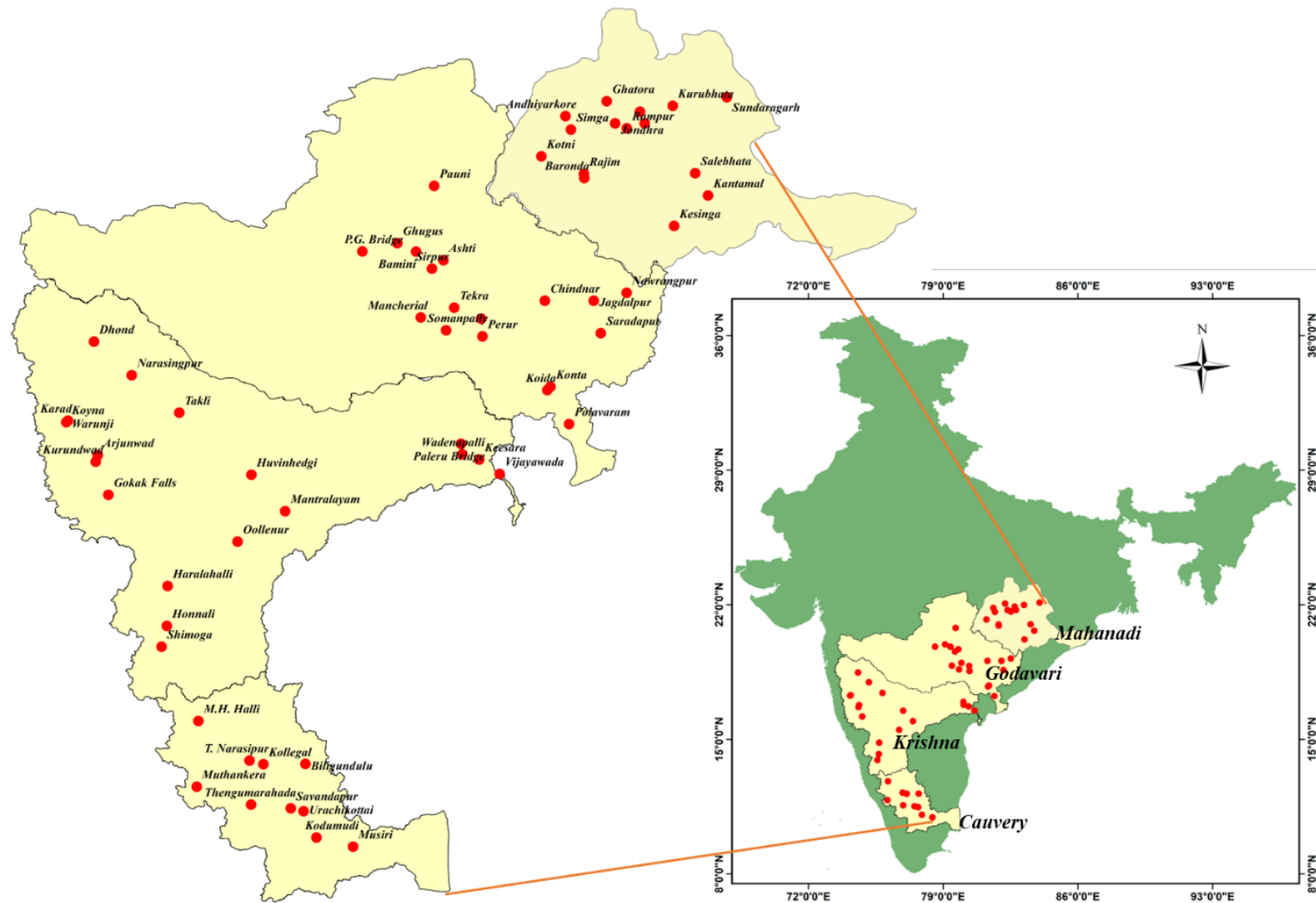
191 The region shown in Fig. 2 is selected as the study area in the Deccan Plateau of Peninsular India. The escarpment
192 of Western Ghats forms the western margin of the Deccan Plateau which serves as the main water divide for the
193 Peninsular River systems. The gentle slope from west to east causes Peninsular rivers such as the Mahanadi,
194 Godavari, Krishna, and Cauvery (Fig. 2) to flow eastwards. Three of these rivers (Godavari, Krishna and Cauvery)
195 originate from the Western Ghats, spread across the area from the Deccan Plateau, flow eastwards, and drain into
196 the Bay of Bengal. The Mahanadi River rises in the mountains of Siwaha bounded by the Eastern Ghats in the
197 south and east, and drain eastwards into the Bay of Bengal. Additional details about the river basins can be found
198 in Text T1 within the Supplementary Information. The study utilizes daily streamflow data (1965-2012) from 62
199 gauges across four river basins, sourced from the Water Resources Information System (WRIS) database. Analysis
200 incorporates a daily gridded rainfall product ($0.25^\circ \times 0.25^\circ$) from the India Meteorological Department (Pai et al.,
201 2014).



202

203 **Figure 1.** (a) The relation of uplift of Himalaya-Tibetan Plateau and monsoon initiation in India. Monsoon winds
 204 blow from the Indian Ocean towards land in the summer (b) during the winter, the Himalaya prevents cold air
 205 from passing into the subcontinent and causes the reversal of wind direction and monsoon blow from land toward
 206 sea [Reprinted from (Chatterjee et al., 2013)] (c) geology of Peninsular India [Reprinted from: Central Ground
 207 Water Board(<https://www.aims-cgwb.org/general-background.php>)].

208



209
 210
 211 **Figure 2.** Location map of four Peninsular River Basins. Stream gauges considered in this study are marked with red circles.

212 **3 Methodology**

213 Initially, the study employs time scale partitioning to analyse flow duration curves across Peninsular India,
214 focusing on Non-monsoon, South-West monsoon, and North-East monsoon periods in four river basins. The
215 analysis extends to regional scales, encompassing streamflow time series from all gauging stations, and includes
216 process scale partitioning to assess the relative contributions of fast and slow flow components, revealing spatial
217 patterns influenced by climate, geology, and aquifer characteristics.

218 Additionally, the methodology entails a comprehensive analysis of FDCs for fast and slow flow components
219 across seasons. It includes scaling time series to remove the influence of mean climate and geology, utilizing the
220 statistical distributions to examine parameters influencing FDC shapes. The study explores links between
221 statistical parameters and landscape properties through recession analysis and investigates spatial variation in
222 FDC parameters using descriptors such as latitude, longitude, and catchment area. The final part of the
223 methodology focuses the association between the midsection slope of the FDC and recession parameters,
224 exploring the role of both surface and subsurface processes in controlling the average flow regime of the
225 catchment.

226 **3.1 Time Scale Partitioning**

227 The streamflow hydrograph, representing a catchment's response to random rainfall events, is treated as a
228 stochastic time series, with streamflow considered a random variable. Utilizing distribution functions like the
229 cumulative distribution function (CDF) allows for a concise assessment of streamflow variability, aiding in the
230 interpretation and comparison of catchment responses. CDFs have diagnostic and practical value, facilitating the
231 classification of catchments based on flow regimes and supporting probabilistic treatments in engineering design
232 and environmental monitoring. The cumulative distribution function of a random variable (the random variable
233 of interest to us is daily streamflow; Q) expresses the probability that a realization (i.e., observation) of Q does
234 not exceed a specific value q .

235 The flow duration curve, an equivalent measure of streamflow variability, represents the fraction of time (D) that
236 streamflow is likely to equal or exceed a specified value, expressed mathematically as,

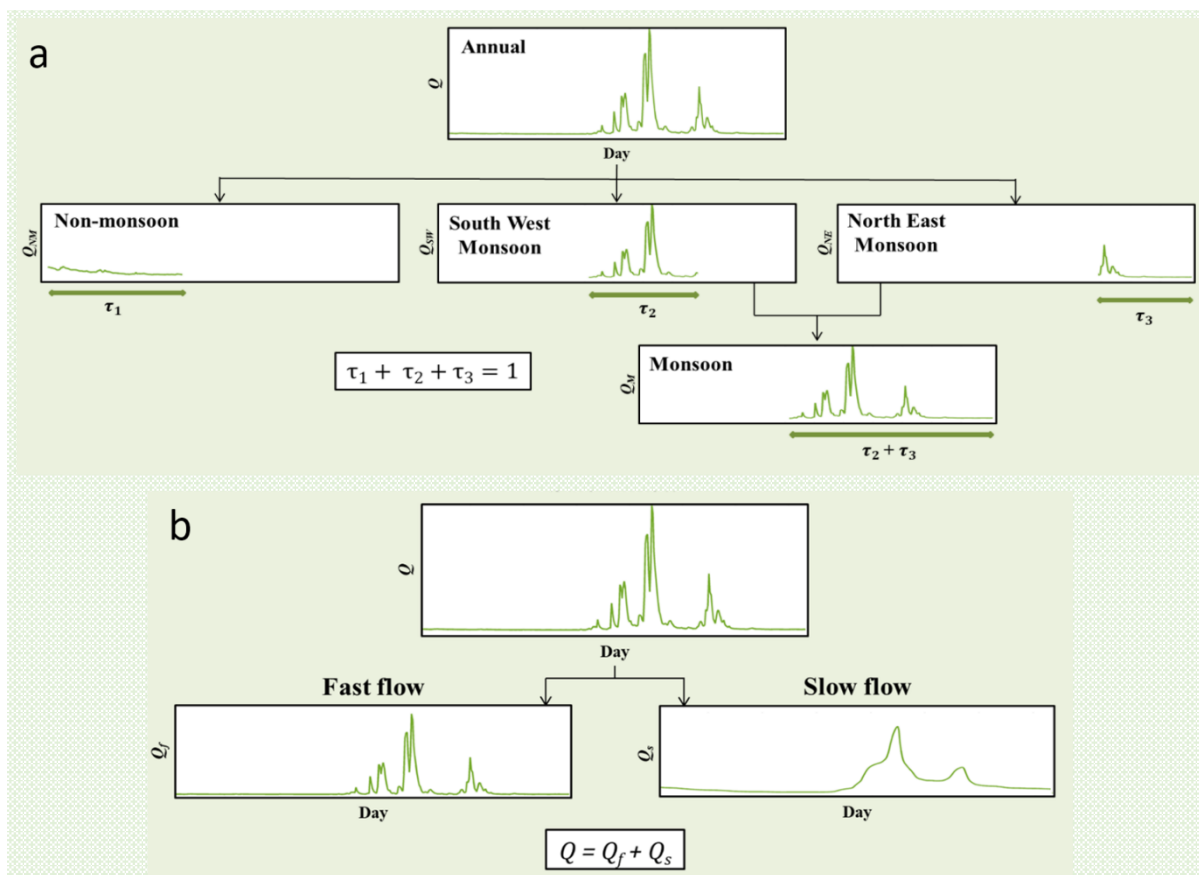
$$D(q) = P[Q \geq q] = 1 - F(q) \quad (1)$$

237 Despite its probabilistic definition, the flow duration curve is commonly plotted in hydrological applications as
238 $q(D)$, i.e., q (in the vertical axis) as a function of D (in the horizontal axis).

239 The streamflow time series can be equivalently divided into temporal segments of distinct seasons as well as
240 distinct months. In this case, by joining observed time series over multiple years, FDCs for each time segment can
241 be reconstructed. Assuming independence (as an approximation), these can then be combined to generate annual
242 FDCs. The theory for the time scale partitioning is illustrated in Fig. 3a. The year is divided into three distinct
243 (non-overlapping) seasons, viz. Non-monsoon, South-West, and North-East seasons (for Peninsular India) of

244 relative durations τ_1 , τ_2 , and τ_3 (with $\tau_1 + \tau_2 + \tau_3 = 1$) respectively. These seasons can be assumed to have
 245 distinct characteristics in terms of rainfall variability and how they translate to streamflow variability. The daily
 246 streamflow time series is used to construct the seasonal as well as annual FDCs. For example, the FDC of Non-
 247 monsoon season is constructed by using the daily streamflow during the period of January – May over the years.
 248 Similarly, FDCs for South-West and North-East monsoons are constructed using the daily streamflow during June
 249 – September and October – December months over the years respectively and the annual FDC is constructed using
 250 daily streamflow values for 365/366 days over the years. The FDCs at monthly time scales are obtained using the
 251 daily values of streamflow in a month over the years. The FDCs for the three distinct seasons, i.e., Non-monsoon,
 252 South-West monsoon, North-East monsoon, are denoted as $D_{NM}(q)$, $D_{SW}(q)$, and $D_{NE}(q)$ respectively. Initially,
 253 the FDCs for each season can be constructed separately (Fig. 3a).

254



255

256 **Figure 3. Time and process scale partitioning. a)** Scale partitioning into seasonal and monthly time scales. The
 257 conceptual framework illustrates the time scale partitioning of streamflow time series into various seasonal
 258 components considering patterns of rainfall variability. The annual streamflow time series is decomposed into
 259 three components: (1) Non-monsoon flow, (2) South-West monsoon flow, and (3) North-East monsoon flow. **b)**
 260 The schematic representation illustrates the process partitioning of streamflow time series into the fast flow and
 261 slow flow components.

262 The annual FDC with exceedance probability $P [Q \geq q]$ refers to the probability of flow in annual scale being
 263 greater than or equal to q , and is expressed as

$$D(q) = P [Q \geq q] = \tau_1 P_{(NM)} [Q \geq q] + \tau_2 P_{(SW)} [Q \geq q] + \tau_3 P_{(NE)} [Q \geq q] \quad (2)$$

$$\text{or, } D(q) = \tau_1 D_{NM}(q) + \tau_2 D_{SW}(q) + \tau_3 D_{NE}(q) \quad (3)$$

264 where, $P_{(NM)} [Q \geq q]$, $P_{(SW)} [Q \geq q]$ and $P_{(NE)} [Q \geq q]$ refer to, respectively, the probability of flow in Non-
 265 monsoon, South-West monsoon and North-East monsoon being greater than q . As the seasons are nonoverlapping
 266 the probability of flow being greater than q at annual scale (i.e., $P [Q \geq q]$) can be expressed as the sum of the
 267 weighted probabilities of flow being greater than q in the three seasons.

268 In general, the FDC at the annual scale can be constructed as follows:

$$D(q) = \tau_1 D_1(q) + \tau_2 D_2(q) + \dots + \tau_n D_n(q) \quad (4)$$

269 where n is the number of distinct seasons considered for the analysis and, $\tau_1 + \tau_2 + \dots + \tau_n = 1$. The validity of
 270 the above depends on the assumption that there is no carryover of flows from one season to the next season (which
 271 is an approximation). In this study, the assumption of independence between flows across three seasons is checked
 272 using multivariate Hoeffding's test (see details in Text T2 of Supplementary Information).

273 The relative contributions of Non-monsoon ($C_{NM \rightarrow AN}$), South-West monsoon ($C_{SW \rightarrow AN}$) and North-East monsoon
 274 ($C_{NE \rightarrow AN}$) flows to annual flow can be approximated through following expressions:

$$C_{NM \rightarrow AN} = \frac{\tau_1 E(Q_{NM})}{\tau_1 E(Q_{NM}) + \tau_2 E(Q_{SW}) + \tau_3 E(Q_{NE})} \quad (5)$$

$$C_{SW \rightarrow AN} = \frac{\tau_2 E(Q_{SW})}{\tau_1 E(Q_{NM}) + \tau_2 E(Q_{SW}) + \tau_3 E(Q_{NE})} \quad (6)$$

$$C_{NE \rightarrow AN} = \frac{\tau_3 E(Q_{NE})}{\tau_1 E(Q_{NM}) + \tau_2 E(Q_{SW}) + \tau_3 E(Q_{NE})} \quad (7)$$

275 Similarly, the relative contributions of monthly flows to annual flow can be expressed as:

$$C_{m \rightarrow AN} = \frac{\frac{1}{12} E(Q_m)}{\frac{1}{12} \sum_{m=1}^{12} E(Q_m)} \quad (8)$$

276 Note, as before, these relative contributions to total flow effectively also measure the relative contributions of the
 277 seasonal/monthly flows to the mean of the annual flow duration curve.

278 The methodology for constructing annual FDC using seasonal FDC is as follows:

279 1. The empirical PDFs – $f_{NM}(q)$, $f_{SW}(q)$ and $f_{NE}(q)$ are derived for daily streamflow time series for Non-
 280 monsoon, South-West monsoon and North-East monsoon seasons respectively.

281 2. These PDFs are then multiplied by scaling factors, τ_1 , τ_2 and τ_3 in equation S4. The scaling factors represent
 282 relative durations of the three seasons considered. For example, $\tau_1 = 5/12$, as the duration of duration of non-
 283 monsoon season is 5 months.

284 3. The PDF of annual flow is estimated as the weighted sum of three scaled density functions corresponding to
 285 three seasons (see Eq. S2). The annual flow consists of the daily streamflow for Non-monsoon, South-West
 286 monsoon and North-East monsoon seasons.

287 The performance of the time scale partitioning framework is assessed using the metric, root mean square error
 288 (RMSE). The method of estimation of q_{sim} is shown in Fig. S3.

$$289 \quad RMSE = \sqrt{\frac{1}{n} \sum_{i=1}^n (q_{actual} - q_{sim})^2} \quad (9)$$

290 **3.2 Process Partitioning**

291 Daily streamflow is partitioned in such a way that it approximates the statistical summation of fast flow and slow
 292 flow at the daily scale (Fig.3b):

$$Q = Q_f + Q_s \quad (10)$$

293 where Q is the daily streamflow, Q_f is the daily fast flow, Q_s is the daily slow flow.

294 The relative contributions of fast flow ($C_{\rightarrow TF}$) and slow flow ($C_{SF \rightarrow TF}$) to total flow can be expressed as

$$C_{Q_f \rightarrow Q} = \frac{\text{Total Fast Flow Volume}}{\text{Total Flow Volume}} \quad (11)$$

$$C_{Q_s \rightarrow Q} = \frac{\text{Total Slow Flow Volume}}{\text{Total Flow Volume}} \quad (12)$$

295 Note that $C_{Q_f \rightarrow Q}$ and $C_{Q_s \rightarrow Q}$ effectively measure the relative contributions of fast and slow flows to the mean of
 296 the annual flow duration curve.

297 **3.3 Exploring Controls and Spatial Patterns of Flow Duration Curves: Insights from Statistical Distributions** 298 **and Analysis of Mid-Section Slope**

299 The analysis then extends to the comprehensive analysis of flow duration curves for fast and slow flow
 300 components across different seasons, with a focus on understanding their variations and controls. The first step is
 301 to scale the fast and slow flow time series by their respective long-term mean values, effectively removing the
 302 influence of mean climate and geology. This scaling allows the identification of secondary controls on the shapes
 303 of FDCs.

304 The Mixed Gamma Distribution (MGD) is then used to fit the scaled fast and slow flow time series, and the
 305 parameters of the MGD are examined for their influence on the FDC shapes (see text T4 of Supplementary

306 Information) Krasovskaia et al., 2006; Botter et al., 2007; Muller and Thompson 2016; Santos et al., 2018. The
307 variation of the parameters of the MGD are explored, regionally and seasonally, considering the influence of mean
308 climate, geology, and complex hydrological processes on fast and slow flows. The performance of the MGD in
309 fitting FDCs is assessed using goodness-of-fit metrics such as the Nash-Sutcliffe efficiency (NSE) and coefficient
310 of determination (R^2). Seasonal variations of MGD parameters are analysed at a regional scale, considering all
311 gauging stations. The studies conducted by Botter et al. (2013), Muller et al. (2014), Basso et al. (2015), Arai et
312 al. (2021), and Leong and Yokoo (2022; 2019) illuminate the complex interplay between recession parameters
313 and FDC characteristics, underscoring the pivotal influence of recession parameters on hydrological systems,
314 encompassing catchment attributes and storage-discharge relationships. Consequently, in pursuit for deeper
315 understanding, we delve into examining the connection between MGD parameters and landscape properties via
316 recession analysis. Spatial variation in FDC parameters is then investigated using descriptors such as latitude,
317 longitude, and catchment area.

318 The final aspect of the methodology involves the association between the midsection slope of the FDC and
319 recession parameters, emphasizing the role of both surface and subsurface processes in controlling the average
320 flow regime of the catchment. The methodology aims to unravel the intricate interplay of climate, geology, and
321 hydrological processes in shaping the regional hydrologic signatures of Peninsular India.

322 **4 Results and Discussions**

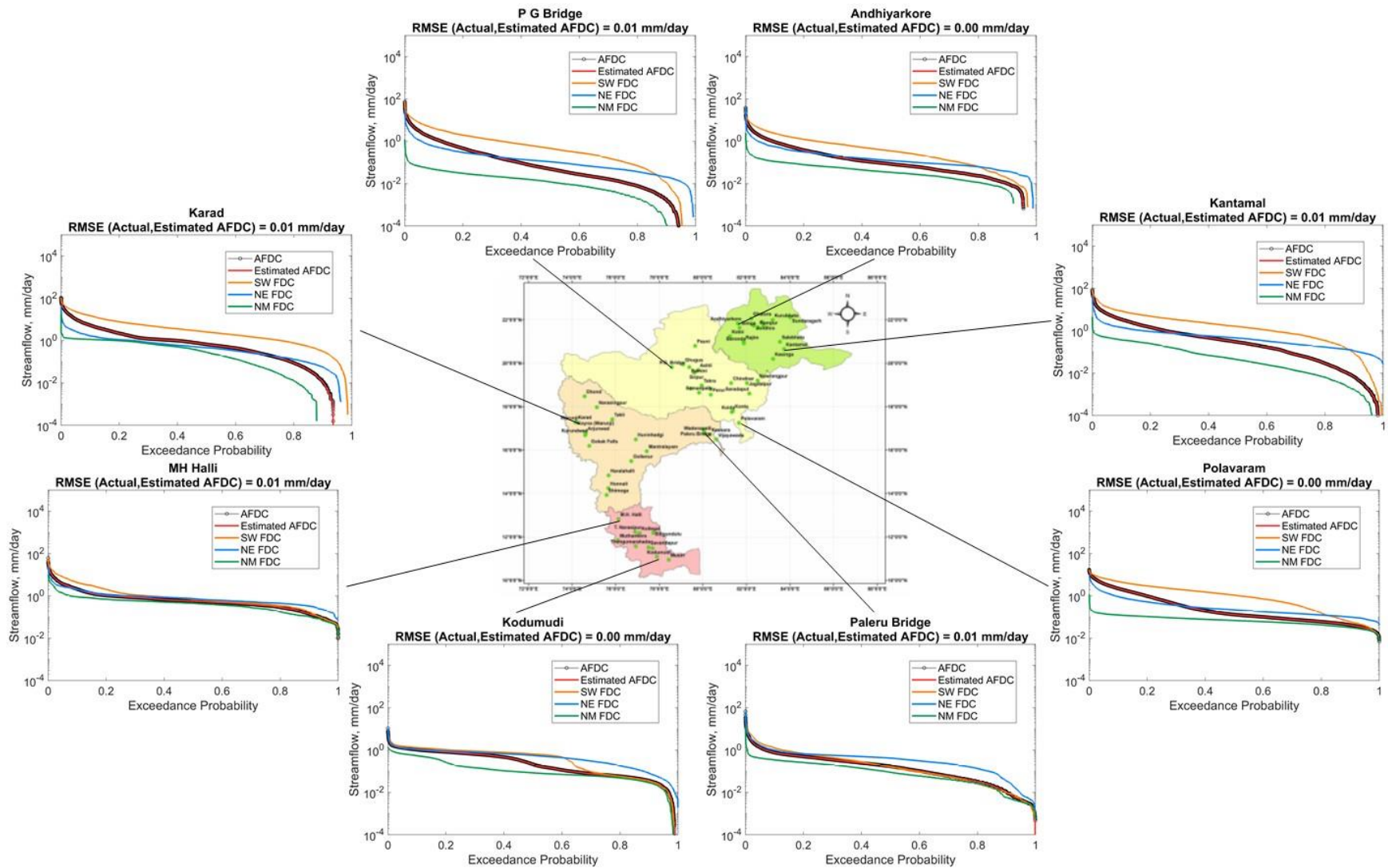
323 **4.1 Time scale partitioning**

324 We initially investigated the spatial variations in seasonal and annual flow duration curves across Peninsular India
325 employing the partitioning framework. The annual flow duration curve and seasonal flow duration curves for
326 Non-monsoon, South-West monsoon, and North-East monsoon are shown in Fig. 4 for eight representative
327 gauges, one at the upstream and one at the downstream of each of the four river basins. The estimated annual flow
328 duration curve (red curve) using equation S2 is also shown in Fig. 4. Daily streamflow time series is normalized
329 by catchment area before plotting (on a semi-log paper) the flow duration curve for comparison across the gauging
330 stations. In particular, the annual flow duration curve (black scatter) is reproduced well by the partitioning of both
331 seasonal (red curve in Fig. 4) and monthly flows (red curve in Fig. S4). The mean and variance of annual flows
332 are also reproduced well by the time scale partitioning framework (Fig. S5). This confirms the efficacy of the time
333 scale partitioning approach of seasonal/monthly flows in approximating the annual flow duration curve (see also
334 Fig. S4, Fig. S5.a and Fig. S5.d in Supplementary Material).

335 Another feature that can be observed in Fig. 4 is that in gauging stations located in the northern part of the
336 peninsular region, flow duration curves (FDCs) of South-West monsoon flows (orange curve) are relatively higher
337 than other seasonal FDCs. Given the logarithmic scale used to plot the flows, this dominance is significant. In
338 sites located in the southern part of the region, the dominance of South-West monsoon is not as strong and North-
339 East monsoon flows (blue curve) are also significant.

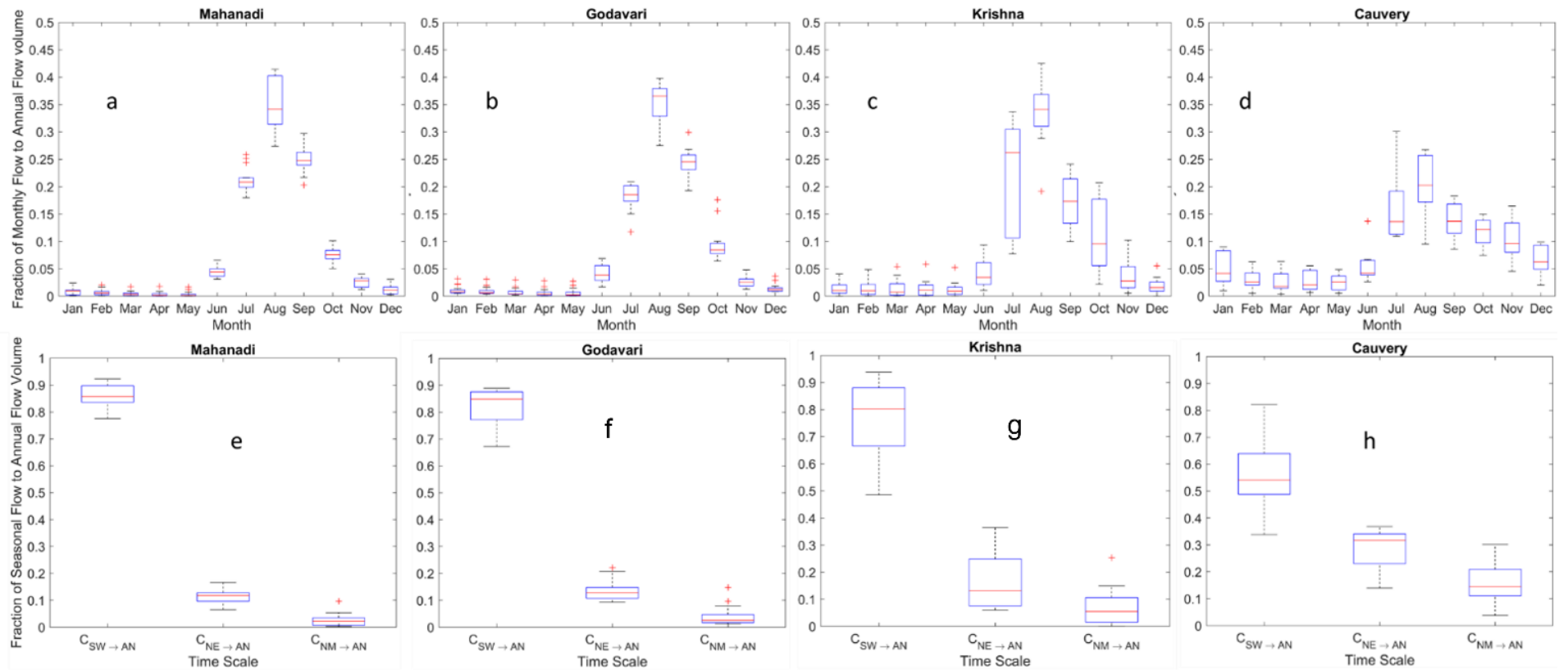
340 Motivated by these observations, we extracted seasonal and monthly streamflow time series from the entire dataset
341 across all gauging stations to compute the relative contributions of seasonal and monthly flows to the annual flow
342 duration curve. The results are presented in Fig. 5. At the monthly scale (top panel, Fig. 5), the contributions of
343 flows during the months of June to September are much higher than in other months in northern Peninsular basins

344 (Mahanadi and Godavari, Krishna to a less extent). This can be explained by the contribution of monthly rainfall
345 to annual rainfall, which is higher during these months as shown in Fig. S6. On the other hand, in the southernmost
346 Cauvery basin, the dominance of June to September months is relatively not as strong, and there is also a
347 significant contribution during the months of October to December, higher than in northern basins (Fig. 5.d). This
348 can be attributed to the slightly more equal dominance of both South-West (June - September) and North-East
349 (October – December) monsoons over the Cauvery basin (Fig. S6.d) than in the northern basins. This pattern is
350 also reflected at the seasonal scale (bottom panel, Fig. 5), with the contribution of South-West monsoon flow to
351 annual flow being slightly higher than that during the other seasons, and much higher in northern basins. However,
352 the contribution of South-West monsoon to annual flow decreases in southern basins, while the contribution of
353 North-East monsoon increases, as can be seen clearly in Fig. 5.h for the Cauvery basin. The contribution of Non-
354 monsoon to annual flow is also higher in southern basins relative to northern basins. This can be attributed to
355 carry over flows from winter rains during the North-East monsoon, which is more pronounced in the southern
356 part of the region.



357

358 **Figure 4.** Spatial variations in seasonal and annual flow duration curves across Peninsular India. The time scale partitioning framework of seasonal flows in approximating
 359 annual flow duration curves works reasonably well.



360

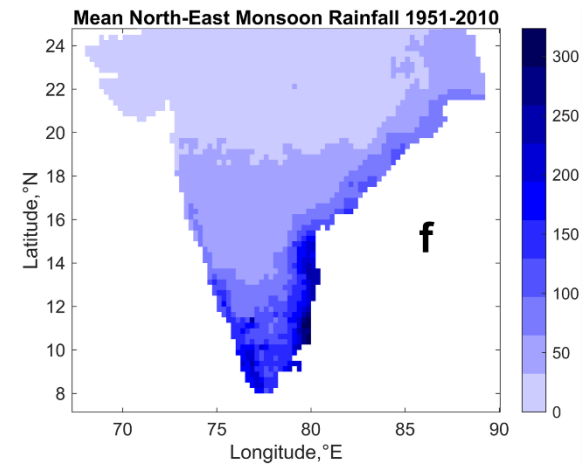
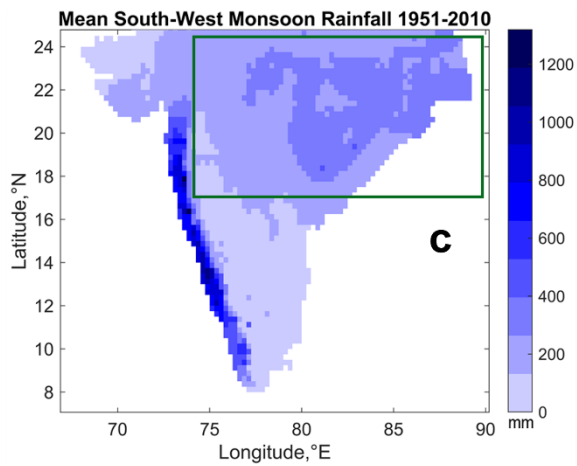
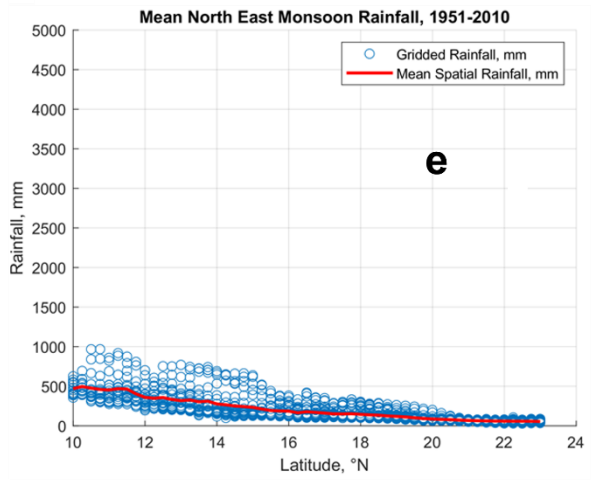
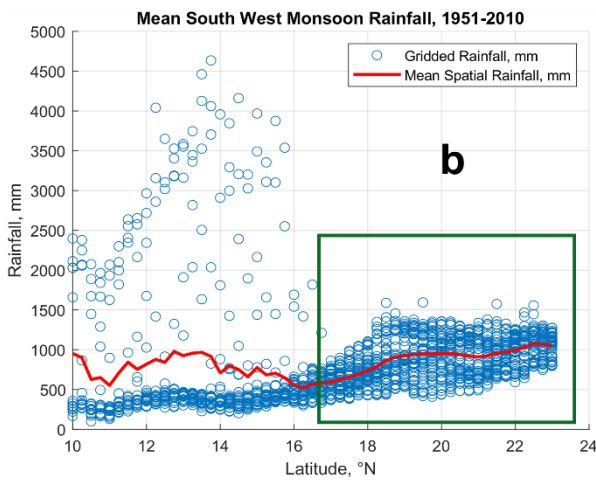
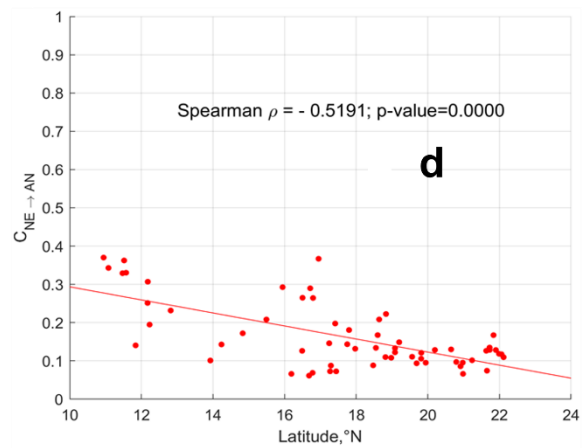
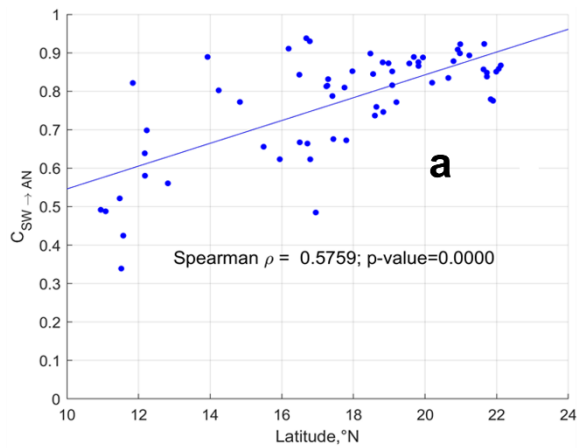
361 **Figure 5.** The relative contributions of monthly and seasonal flows to annual flow at basin scale. The contributions of South-West monsoon flow to annual flow increases in
 362 northern basins whereas it decreases in southern basins. However, the contributions of North-East monsoon flow to annual flow increases towards southern basins.

363 We next carried out regional scale analysis by considering streamflow time series of all the gauging stations across
364 all four river basins. Similar to basin scale analysis presented before, the relative contributions of seasonal and
365 monthly flows to annual flow are now estimated at the regional scale (Fig. 6). The spatial patterns of South-West
366 and North-East monsoon rainfall across the Peninsular region are plotted for comparison using IMD gridded
367 rainfall product (Fig. 6.b and Fig. 6.e).

368 The contribution of South-West monsoon flows to annual flow increases in the northerly direction (Fig. 6.a). The
369 mountainous region of the southern Peninsula (western part of Krishna basin and north-western part of Cauvery
370 basin) receives high rainfall during the South-West monsoon season (Fig. 6.b – extended till 17° N latitude). The
371 streamflow produced in the headwater regions of southern basins in response to high rainfall, contributes at least
372 70% of the annual flow (Fig. 6.a). Yet, the areal fraction of these high rainfall, headwater regions within the four
373 river basins is quite small and their contributions to the average precipitation or flow at the basin scale is much
374 smaller. There is also considerable variability in the contributions of South-West monsoon flows to annual flow
375 in the sub-basins located at the eastern and south-eastern parts of Krishna and Cauvery basins (represented by the
376 scatter below the regression line till 17° N latitude in Fig. 6.a) due to declining rainfall (Fig. 6c). This considerable
377 variability, on average, reduces the overall contributions of South-West monsoon to annual flow in southern
378 Peninsula with respect to the basins in the northern part.

379 The northern part of the Peninsular region receives comparatively higher rainfall than the southern part without
380 considering the Western Ghats. This increased rainfall is attributed to the movement of low-pressure systems that
381 develop over the Bay of Bengal towards central India (Krishnamurthy & Ajayamohan, 2010; Prakash et al., 2015).
382 The low-pressure systems are a regular feature of South-West monsoon, which brings significant amount of
383 rainfall in the northern part of the Peninsular region (Krishnamurthy & Ajayamohan, 2010). The increased rainfall
384 (Fig. 6.b – after 16° N latitude) is responsible for higher contribution of South-West monsoon flows to annual
385 flow in the northern basins. As the spatial variability of this rainfall is comparatively less than in the southern
386 Peninsular region, there is less variability in the contribution of South-West monsoon flows to annual flow. The
387 spatial variability in South-West monsoon along the south-north direction across Peninsular region can explain
388 the gradient in the contribution of South-West monsoon flows to annual flow in the same direction.

389 On the other hand, the contribution of North-East monsoon flows to annual flow increases in the southerly
390 direction (Fig. 6.d and Fig. 6.e). This can be explained by the fact that the southern part of the Peninsular region
391 receives higher rainfall during North-East monsoon than the rest of the Peninsular region (Fig. 6.f).



392

393 **Figure 6.** Contribution of seasonal flows to annual flow at regional scale. The spatial variability of South-West
 394 and North-East monsoons can explain the variation in contributions of seasonal flows to annual flow across south-
 395 north gradient. The green box in (b) indicates the northern part of peninsular region which receives higher rainfall
 396 than the southern part. The green box in (c) indicates the spatial extent of the rainfall grids which was considered
 397 in figure (b). The red line in figure (b) indicates the mean rainfall – obtained by averaging the rainfall values at a
 398 specific latitude (°N).

399 The application of the analysis framework used here is based on the critical assumption of independence of flows
400 between different seasons (months), which needs to be critically evaluated. Moisture carry-over across seasons is
401 a confounding issue in the case of strongly seasonal catchments (i.e., exhibiting sharp transition from wet season
402 to dry season in terms of rainfall climatology), specifically when the initial wetness condition at the onset of the
403 dry season depends on the final wetness at the end of wet season and vice-versa. Although most of the rainfall
404 (58-90%) is concentrated during South-West monsoon months (i.e., June – September, red bar in Fig. S7) in
405 Peninsular basins, more than 10% of the annual rainfall is received during North-East monsoon months (i.e.,
406 October – December, yellow bar for Cauvery and Krishna in Fig. S7). In addition, more than 8% of annual rainfall
407 occurs in non-monsoon season (i.e., January – May, blue bar in Fig. S7). This highlights that rainfall received
408 during non-monsoon and North-East monsoon seasons are comparable, and thus it is difficult to distinguish the
409 rainfall climatology across these seasons. Therefore, it is challenging to declare these are catchments with
410 seasonally dry climates. In order to justify our assumption in the reconstruction of annual FDC from seasonal
411 flows, we have now conducted a multivariate Hoeffding test (Gaißer et al., 2010) to check the independence
412 between three random variables representing Non-monsoon, South-West Monsoon and North-East Monsoon
413 flows respectively. A value of test statistic – φ^2 – close to zero indicates independence between three random
414 variables. It is observed that except for two stations in Krishna basin, 60 out of 62 stations show independence
415 between flows across the seasons (Fig. S8). This supports appropriateness of the assumption of no carry-over that
416 had been used in this study to construct annual FDC based on seasonal FDCs.

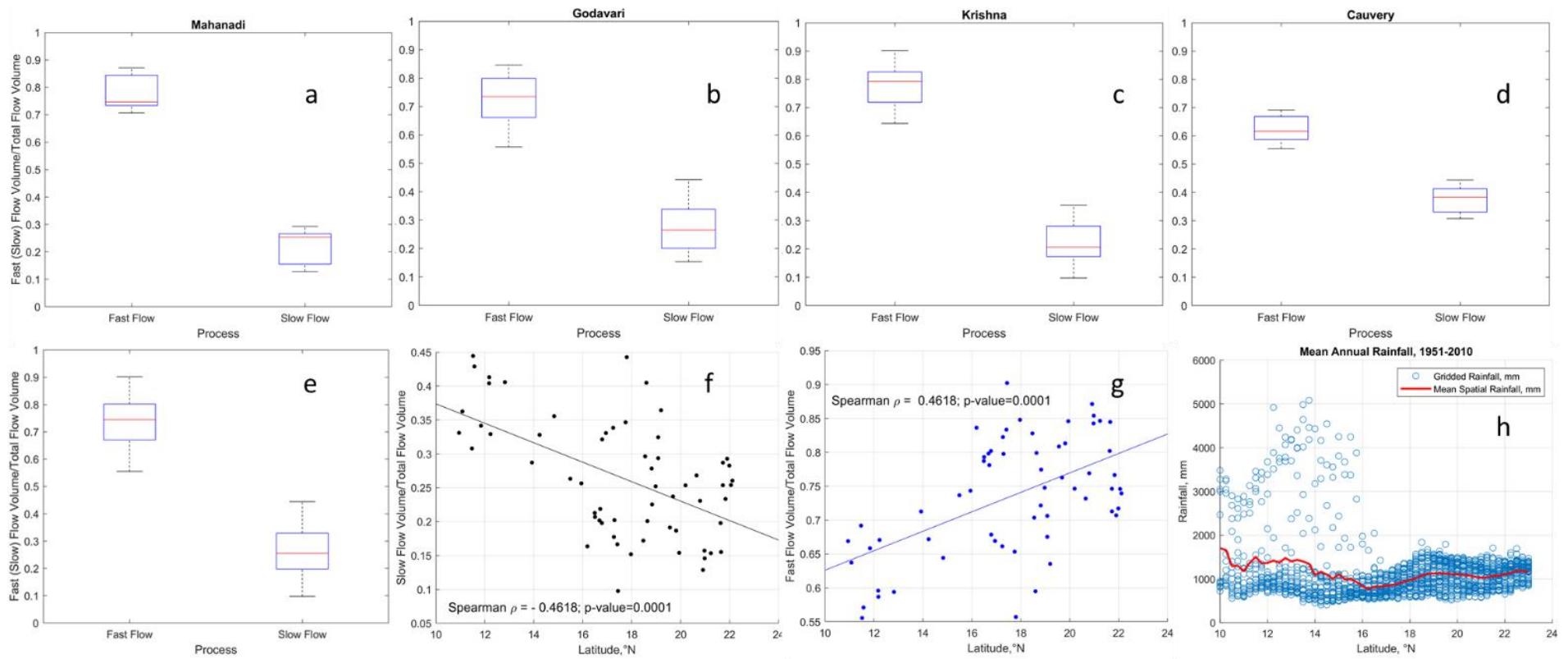
417 **4.2 Combined influence of time scale and process scale partitioning**

418 In order to further explore the climatic and landscape controls of streamflow variability regionally, we next
419 partition streamflow into fast and slow flow components, notionally representing surface runoff, and a
420 combination of subsurface and groundwater flow respectively (Ghotbi et al., 2020a, b). Fast flow is controlled by
421 event scale runoff generation processes and its variability is characterized by topography, land use, soil and rainfall
422 characteristics. On the other hand, climate seasonality and geologic formations of the subsurface are primary
423 controllers of slow flow variability (Ghotbi et al., 2020a, b). The slow flow component is extracted from observed
424 streamflow by using a recursive digital filter (see details in Text T5 of Supplementary Information). The fast flow
425 component is obtained by then subtracting the slow flow from observed streamflow. The relative contributions of
426 fast flow and slow flow to total flow (and hence also mean annual flow) are estimated using equations 11 and 12
427 respectively, for all the gauging stations across all four basins. The relative contributions of fast and slow flows
428 to total flow at the basin and regional scales (combining all the gauging stations) are shown in Fig. 7. In addition,
429 the long-term mean annual rainfall across the Peninsular region is also presented for comparison and to possibly
430 explain the contributions of fast flow (Fig. 7.h).

431 The contributions of fast and slow flows to total flow in each of the four river basins is presented in Fig. 7.a to
432 Fig. 7.d, indicating a strong dominance of fast flow in the northern basins (close to 80% in Mahanadi, Godavari
433 and Krishna), and relatively less dominance (around 60%) in the southern Cauvery basin. This dominance of fast
434 flow also shows up at the regional scale (Fig. 7.e). The regional variations of the relative contributions of slow
435 and fast flows to total flow can also be seen in the results for individual gauges presented in Fig. 7.f and Fig. 7.g,
436 respectively. On average, the contribution of slow flow decreases in the northerly direction, while the contribution
437 of fast flow increases in a corresponding way.

438 The contribution of fast flow to total flow increases in the northern direction of the Peninsular region (Fig. 7.g).
439 The fast flow component of streamflow is generally more responsive to the characteristics of rainfall intensity.
440 The southern part of the region receives high rainfall over Western Ghats along the western edge of Krishna basin
441 and Cauvery basin (Fig. 7.h). In Cauvery basin, the headwater catchments (namely, MH Halli, Muthankera and
442 Thengumarahada in Fig. S6) contribute 57 – 65 % of fast flow to total flow locally. The subbasins located at the
443 western edges of Krishna basin contribute 80% of the fast flow to total flow (between 13° N and 18°N latitudes
444 in Fig. 7.g) locally. However, there is a wide range of variability in the contributions of fast flow to total flow for
445 subbasins located in the eastern part of Krishna basin. The spatial mean rainfall increases and variability decreases
446 after 16° N latitude (Fig. 7.h), which dictate the increased contribution fast flow to total flow. Therefore, the
447 spatial characteristics (mean and variability) of annual rainfall control the south-north gradient in fast flow
448 contributions to total flow. In order to explain the variability in slow flow fraction of total flow, a multivariate
449 regression analysis is performed (details are provided in Text T8). It is observed that the location of the gauges is
450 an important predictor of the slow flow fraction of total flow in Peninsular region, revealing the existence of
451 regional groundwater gradient in the region (Table T1). In addition to the location of the gauges, the recession
452 parameter, β – that controls the aquifer geometry and water level elevation profile during early and late stages of
453 recession – is found to be significant in explaining the slow flow fraction of total flow (Table T1).

454 The contributions of slow flow to total flow increases in the southerly direction over the Peninsular region (Fig.
455 7.f). This can be explained by two major factors. Firstly, the Peninsular region is mostly dominated by hard rock
456 geologic formations, where the subsurface flows are controlled by secondary porosities due to weathering and
457 fracturing (Chandra, 2018; Das, 2019). The distribution of these formations is highly heterogenous (Fig. 1.c) and
458 is responsible for baseflow (slow flow) contribution to total flow (Collins et al., 2020; Narasimhan, 2006). For
459 example, 84% of the total area of Cauvery basin is classified as moderate and good groundwater potential zone
460 (Arulbalaji et al., 2019). The influence of such potential regions of Cauvery basin is reflected on the presence of
461 significant amount of slow flow even in the Non-monsoon season (Fig. 8.g and Fig. 8.h). Likewise, 63% of the
462 total area of Krishna basin is classified under same category (Harini et al., 2018). However, the slow flow regime
463 becomes much more seasonal (Fig. 8) in the northern part of the Peninsular region due to limited capability of
464 geologic formations in transmitting slow flow (Patil et al., 2017) as well as strong seasonality in rainfall patterns
465 (Fig. 8). Secondly, the southern part of the Peninsula receives rainfall almost equally during both South-West and
466 North-East monsoons, which is reflected in the bimodal pattern of rainfall seasonality (Fig. 8.g and Fig. 8.h). The
467 compounding effect of bimodal rainfall seasonality and higher fraction of moderate to good groundwater potential
468 zones explains the higher contribution of slow flow to total flow in southern part of the Peninsular region.

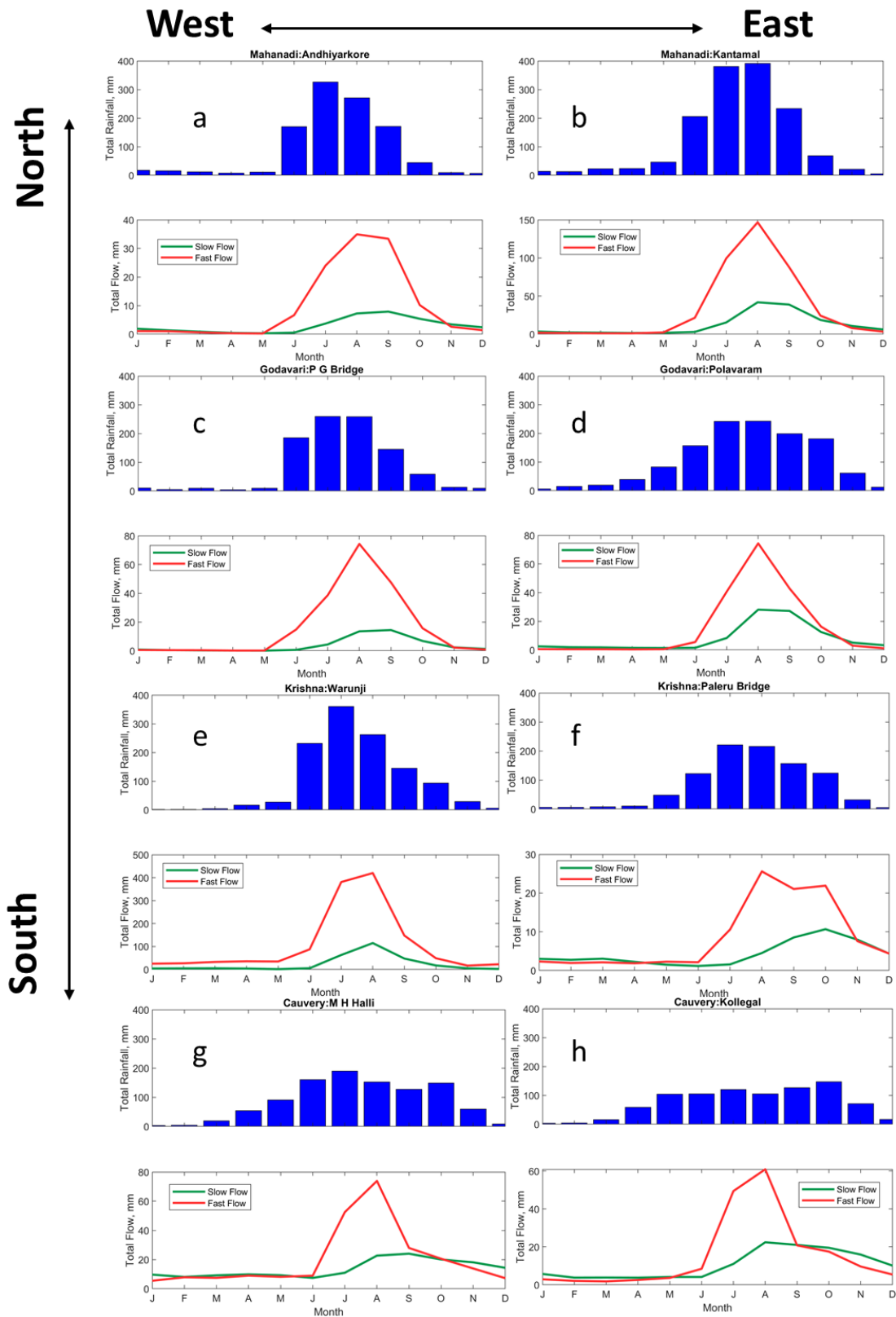


470

471 **Figure 7.** Relative contributions of fast and slow flow to total flow. Consistent higher contribution of fast flow and lower contribution of slow flow to total flow are observed
 472 in Peninsular India (a – d) at basin scale. At regional scale, a systematic gradient in fast and slow flow contributions is observed (f and g). The spatial patterns of rainfall (h)
 473 can explain the gradient in fast flow contributions. The high scatter of rainfall in the low latitudes represents the heavy rainfall with high variability occurring in the Western
 474 Ghats.

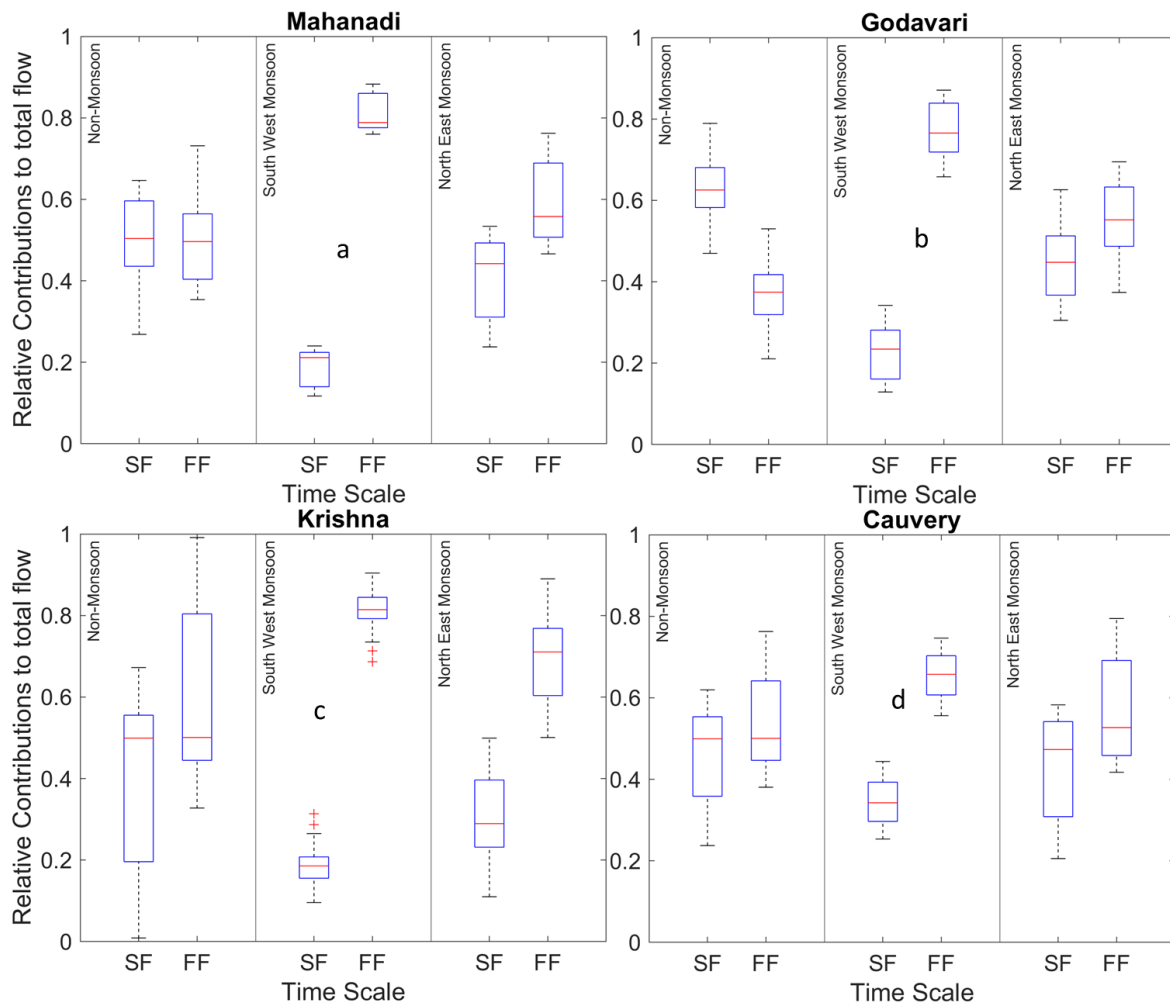
475 Further, an investigation of the combined influence of climatic time scales and process time scales is therefore
476 pertinent to fully understand the controls of streamflow variability in this region. To address this question, we
477 extracted the fast and slow flow components for each of the Non-monsoon, South-West monsoon and North-East
478 monsoon seasons. These components are then used to estimate their relative contributions to total flow for the
479 three seasons across all the gauging stations.

480 The relative contributions of fast and slow flow to total flow at basin scale are shown in Fig. 9. It is observed that
481 during the Non-monsoon period, the median contributions of fast and slow flow for Mahanadi, Krishna and
482 Cauvery basins are similar, although there exists considerable variability in their distribution. With the onset of
483 the South-West monsoon, the contribution of fast flow to total flow increases markedly for all the basins, although
484 relatively much less in the Cauvery basin. During the subsequent North-East monsoon season, the contribution of
485 fast flow decreases whereas slow flow contribution increases. The fluctuations in the fast flow contributions can
486 be explained by the onset and withdrawal of the monsoon seasons, which are major contributors to fast flow
487 generation. The fluctuations in the fast flow contributions across seasons can be explained by the differences in
488 the rainfall amount during South-West and North-East monsoons (Fig. 6.c and Fig. 6.f). Among all four basins,
489 the difference in median contributions of fast and slow flow is minimum. These can be attributed to the presence
490 of higher fraction of moderate and good groundwater potential zones (Arulbalaji et al., 2019) which promotes
491 baseflow even in dry periods (Fig. 8.g and Fig. 8.h). The presence of bimodal pattern in rainfall seasonality due
492 to both South-West and North-East monsoons minimizes the difference between the relative contributions of fast
493 and slow flow to total flow.



494

495 **Figure 8.** Spatial variation of long-term monthly fast and slow flow components of streamflow at selected gauges
 496 in Peninsular region. The blue bar plots represent the long-term monthly rainfall averaged over the sub-basins
 497 corresponding to the gauging stations. The seasonality in rainfall patterns changes (unimodal to bimodal) across
 498 north-south direction of the Peninsular region.



499

500 **Figure 9.** Seasonal contributions of fast (FF) and slow flow (SF) to total flow at basin scale.

501

502 **5. Stratification of streamflow variability**

503 **5.1 Understanding physical controls and spatial variation of flow duration curve by fitting statistical**
 504 **distributions**

505 So far in this paper, in order to understand the physical controls on regional streamflow variability across
 506 Peninsular India we have partitioned observed streamflow in two ways: (i) seasonal/monthly flows, and (ii) slow
 507 and fast flows. We looked at the relative contributions of these components to mean annual streamflow, looked at
 508 how the relative contributions varied regionally, and attributed these to the relative strengths of the monsoons and
 509 spatial variations of geological formations. We now return to the FDCs of the flow components, especially the
 510 shapes of the FDCs (as reflected in the parameters of the fitted distribution) and look at how they themselves vary
 511 regionally.

512 In our study the fast and slow flow time series are scaled by their respective long-term mean values to remove the
 513 influence of mean climate and geology, thus providing an opportunity to identify the secondary controls on the
 514 variation of shapes of FDCs. The scaled fast and slow flow time series are now used to fit the mixed gamma
 515 distribution (MGD, (see details in Text T4 of Supplementary Information). The parameters of mixed gamma

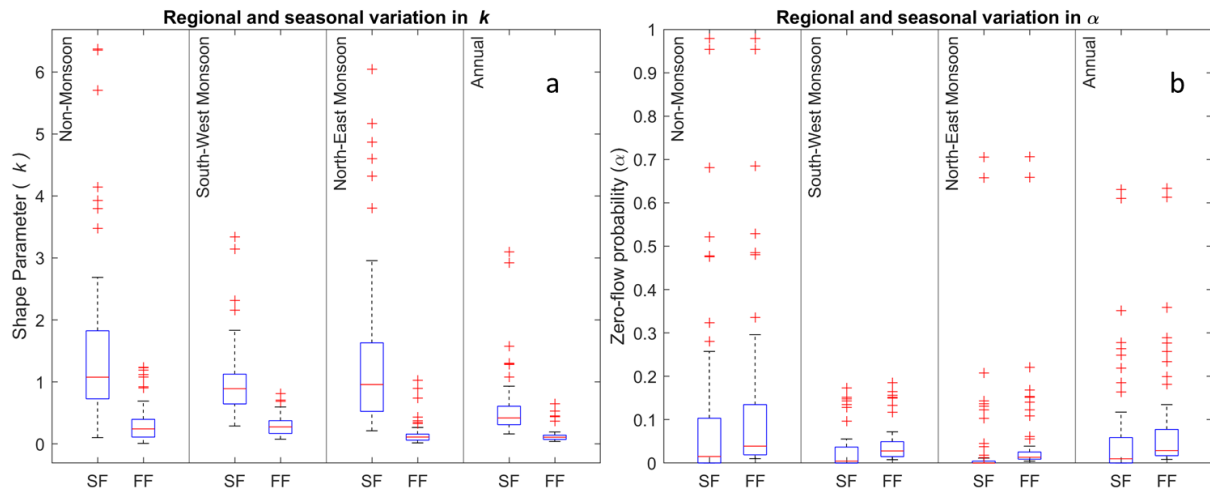
516 distribution control the shape and orientation of the FDC. For example, the shape parameter k controls the slope
517 of the FDC whereas α controls the zero-flow part of the FDC. However, the parameter θ affects the vertical shift
518 of the FDC. In addition, these parameters are also linked with the mean and variance of the streamflow time series.
519 For example, the scale parameter θ is directly proportional to the mean of the time series whereas, the shape
520 parameter k is inversely proportional to the variance of the time series.

521 As the fast and slow flow time series are scaled with their respective long-term means, the scale parameter (θ) is
522 approximately found to be inversely proportional to shape parameter (k) through the relationship, $k\theta = \frac{1}{1-\alpha}$
523 (Cheng et al., 2012). Therefore, the variations of only k and α – zero-flow probability, are presented in this section.
524 The variation of k can be related to the steepness of the FDC, i.e., smaller values of k will have steeper slopes.

525 The Nash-Sutcliffe efficiency (NSE) and coefficient of determination (R^2) goodness of fit of fast/slow flows to
526 MGD is shown in Fig. S10 (in Supplementary Information). In addition, the observed and simulated fast and slow
527 flow FDCs are compared in Fig. S8 (in Supplementary Information). It is observed that the slow flow component
528 fits well to mixed gamma distribution than fast flow component, as slow flow is most stable component and MGD
529 satisfactorily captured the shape of slow flow FDC. However, MGD adequately captures the shape of fast flow
530 FDCs at upper tail (high flow segment), except for the lower tail (low flow segment). The fast flow processes are
531 governed by more complex processes (for example, infiltration and saturation excess runoff generation, runoff
532 routing, stochastic nature of storm events, properties of soil and topography etc.) than slow flow (for example,
533 climate seasonality and underlying geology of aquifer system).

534 The seasonal variation of parameters of the mixed gamma distribution at regional scale (comprising of all the
535 gauging stations) is presented in Fig. 10. The mixed gamma distribution performed well in fitting the flow duration
536 curves of two flow components across different seasons (Fig. S10). In Fig. 10.a, it is observed that the shape
537 parameter of slow flow is consistently higher than that of fast flow. The shape parameter is inversely proportional
538 to the variance of streamflow. The slow flow exhibits lower variance due to its longer time of residence in the
539 subsurface formations. Moreover, the subsurface formations in Cauvery River basin are more favourable to slow
540 flow in comparison to the other three basins (Fig. 8.g and Fig. 8.h). In addition, the bimodal seasonal pattern of
541 rainfall is also responsible for occurrence of slow flow even in the Non-monsoon period for the southern basins
542 (Fig. 8).

543 The fast flow component exhibits higher variance than the slow flow component. The median shape parameter of
544 fast flow is highest during South-West monsoon season and lowest during North-East monsoon (Fig. 10.a). This
545 can be explained by the lower variance of fast flow during South-West monsoon as the rainfall amount is higher
546 during the season compared to the North-East monsoon (Fig. 6.c and Fig. 6.f). The dominance of both South-
547 West and North-East monsoons in Cauvery basin results in lower variance of fast flow compared to the northern
548 basins. The fast flow duration curves are steeper than the slow flow duration curves for all seasons, as the
549 magnitudes of k for fast flow are smaller than that of slow flow (Fig. 10.a).



550

551 **Figure 10.** Regional and seasonal variation of k and α parameter of mixed gamma distribution.

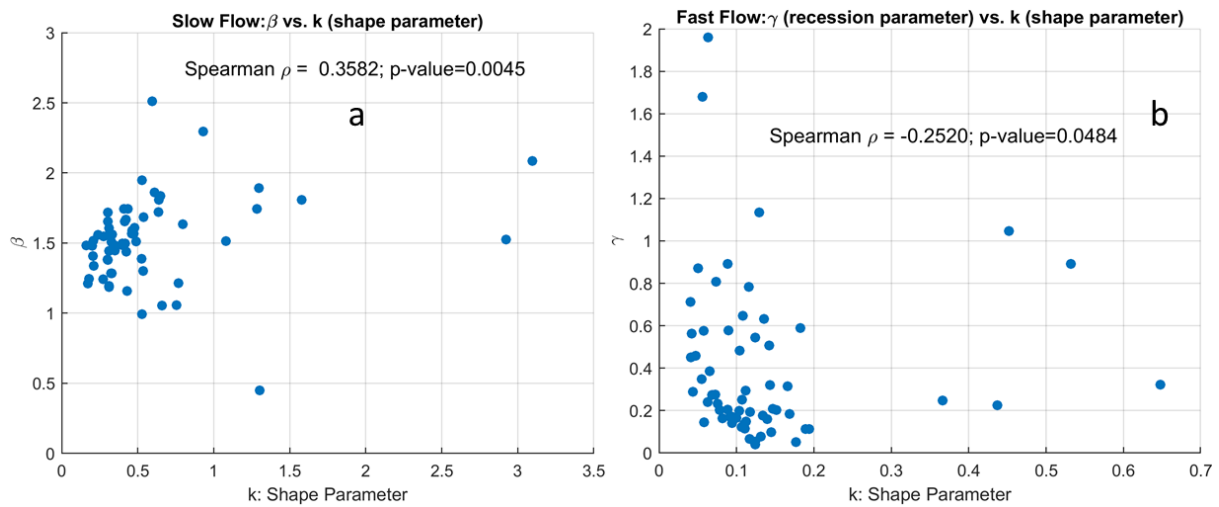
552 The parameter α controls the zero-flow part of the flow duration curve. It is observed that the mean α for slow
 553 flow is minimum during South-West monsoon and maximum for Non-monsoon season (Fig. 10.b) on a regional
 554 scale. This can be attributed to the combined influence of rainfall during South-West monsoon and the
 555 connectivity between underlying geologic formations in the Peninsular region. For the fast flow, the mean α is
 556 minimum during the South-West monsoon and maximum during Non-monsoon as the South-West monsoon is
 557 the dominating rainfall season in Peninsular India.

558 The shape parameters (k) of MGD for slow and fast flow components are linked with landscape properties through
 559 recession analysis, where the parameters γ and β of power-law relationship are estimated using streamflow data
 560 (details in Text T6 in Supplementary Information). It is observed that shape parameter (inversely proportional to
 561 variability) of slow flow is positively correlated with β . The parameter β is influenced by aquifer geometry and
 562 water table elevation profile defining early and late stages of recession (Tashie et al., 2020a; Tashie et al., 2020b).
 563 Higher values of β indicate slow late recessions which is characterized by low variability in slow flow (Fig. 11.a).

564 The shape parameter of fast flow is negatively correlated with the parameter γ of the power-law relationship (Fig.
 565 11.b). The parameter γ strongly related with the seasonality of catchment wetness and evapotranspiration which
 566 are primary governing factors for runoff generation (Dralle et al., 2015; Gnann et al., 2021). In addition, the spatial
 567 variation of rainfall also influences the variability of γ (Biswal & Kumar, 2014) which reflects the variability of
 568 fast flow.

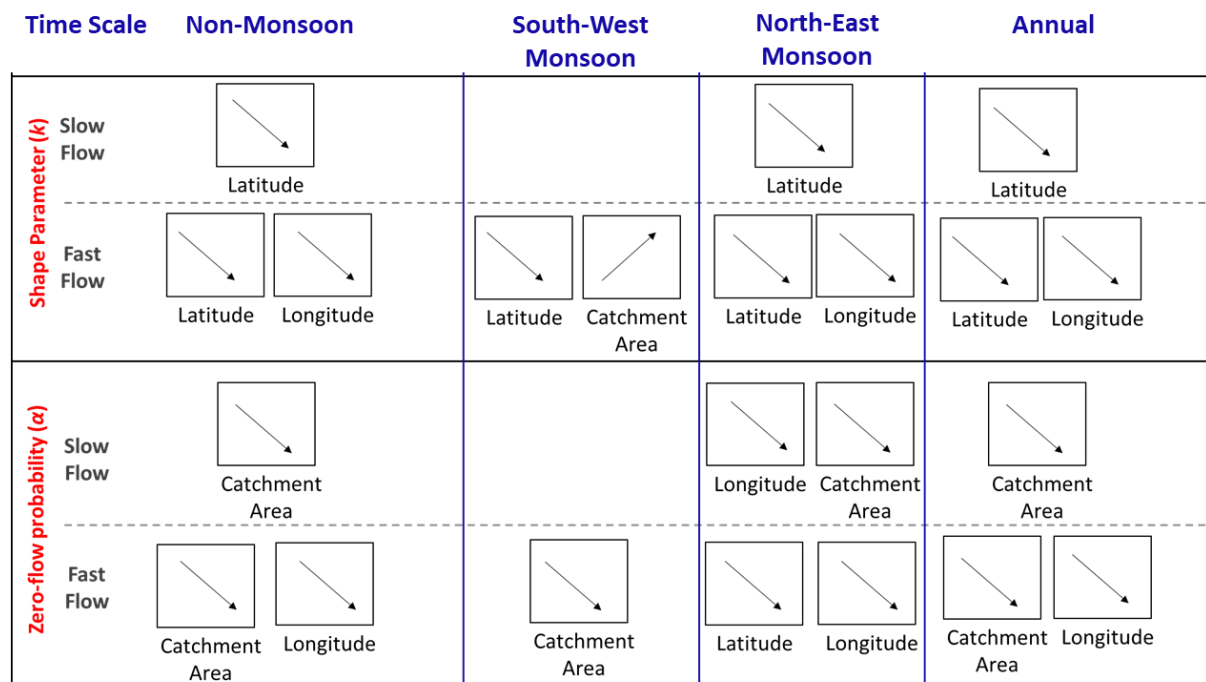
569 The variation of the parameters, k and α was also studied using spatial descriptors (latitude and longitude) as
 570 explanatory variables to understand the spatial variation of FDCs across south-north, west-east gradients. In
 571 addition, the behaviour of these parameters is also assessed using catchment area as another explanatory variable.
 572 The regional parameter sets comprising of k and α are next constructed for slow and fast flow processes by
 573 including these parameters for all the time series across different gauging stations across the Peninsular region.
 574 The Spearman correlation coefficients between these parameters and explanatory variables (i.e., catchment area
 575 and spatial descriptors – latitude and longitude) for slow and fast flow processes at seasonal scales are computed.

576 The schematic representation of significant directions (positive/negative correlations) in Spearman coefficient is
 577 shown in Fig. 12.



578

579 **Figure 11.** Relationship between flow variability (related inversely to shape parameter, k of mixed gamma
 580 distribution) and recession parameters.



581

582 **Figure 12.** Schematic representation of spatial and temporal variation of parameters of mixed gamma distribution
 583 across Peninsular India. The direction of significant Spearman correlation coefficient between model parameters
 584 and descriptors (catchment area and spatial descriptors – latitude and longitude) for fast and slow flow across
 585 multiple time scale is presented.

586 The shape parameter of fast flow is found to be positively correlated with catchment area (Fig. 12, top panel),
 587 implying lower variability of fast flow in large catchments. This can be attributed to increased smoothing effect
 588 of incoming rainfall in larger catchments through various storages, thus reducing the variability of fast flow.
 589 Moreover, the shape parameters for fast flow are negatively correlated with spatial descriptors, indicating

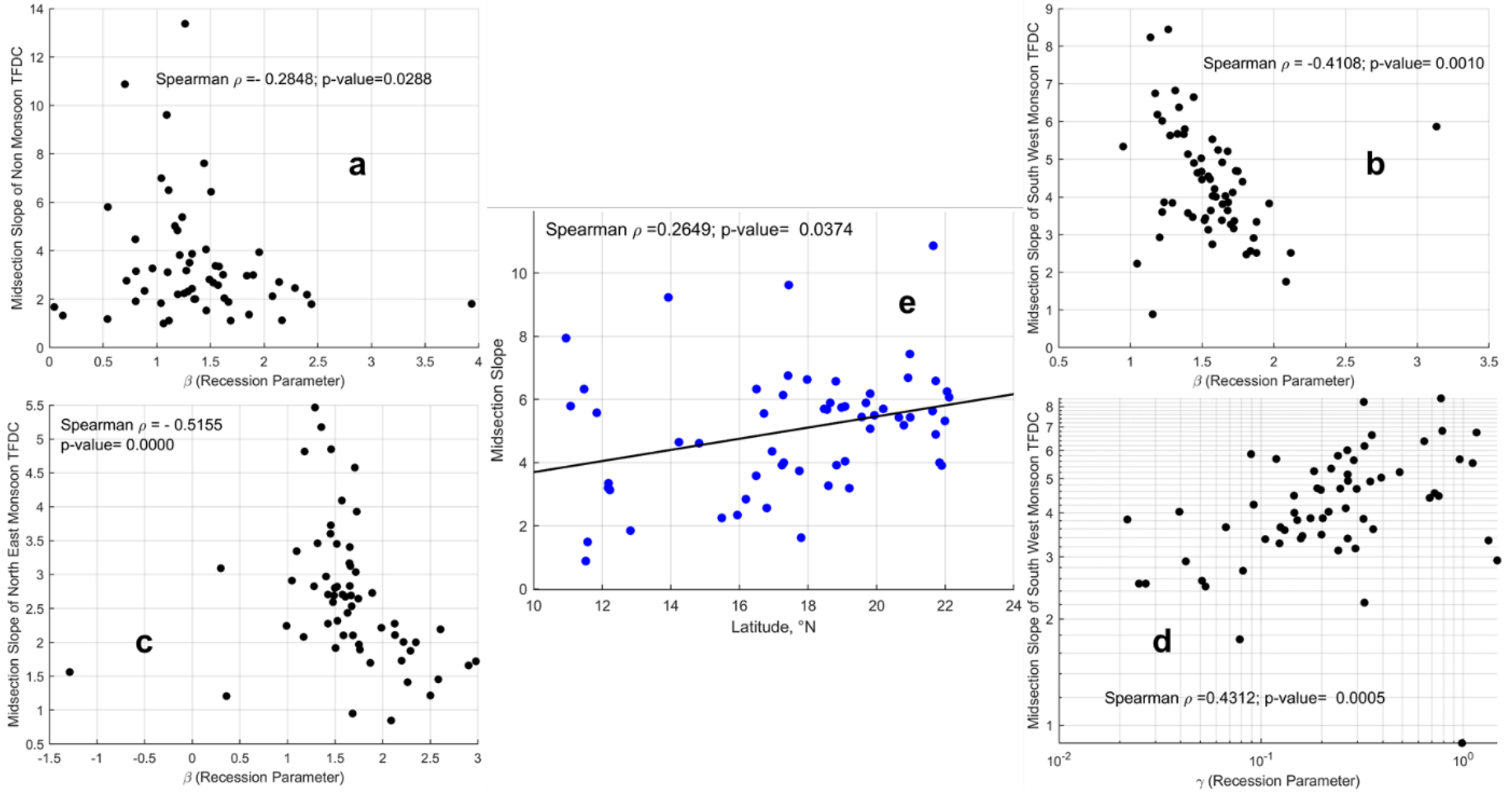
590 increased variability of fast flow along south-north and west-east gradients. This can be partly explained by the
591 bimodal seasonal pattern of rainfall due to dominance of South-West and North-East monsoons, thus reducing the
592 variability of fast flow in the southern part of the region. The rainfall pattern becomes more seasonal (primarily
593 due to South-West monsoon) in the northern part of region which can contribute to increased variability of fast
594 flow. The presence of numerous water retention structures for supporting irrigation in these regions (54 – 75% of
595 Peninsular basins are crop land) can modify the variability of the flow, although we have not analysed this
596 separately in this study.

597 The shape parameter of slow flow is found to be negatively correlated with latitude, implying that slow flow
598 becomes highly variable in the northern part of the region. This can be explained by the nature of geologic
599 formations in the Cauvery basin that promotes slow flow even during the Non-monsoon period. However, in the
600 northern part of the region, the slow flow tends to become more seasonal and has very limited flow during non-
601 rainy seasons. In addition to the geology, the bimodal seasonal rainfall patterns due to monsoons can play an
602 important role in the variability of slow flow. Apart from the spatial descriptors, the slow flow variability is
603 inversely proportional to catchment area, implying larger catchments have lower slow flow variability than
604 smaller catchments. This can be explained by the proportional increase in area of contribution to slow flow with
605 increase in catchment size, thus reducing the variability in slow flow for larger catchments.

606 The parameter α is found to be negatively correlated with catchment area (Fig. 12, bottom panel) for fast and slow
607 processes, implying zero-flow probabilities are lower for larger catchments. The higher residence time of water
608 in larger catchment due to various kinds of storages facilitates flow in river even in Non-monsoon season, thus
609 reducing the zero-flow probabilities. In addition, the parameter α of both slow and fast flow are negatively
610 correlated with longitude, implying lower zero-flow probabilities along west-east direction. This can be attributed
611 to natural declining elevation (Fig. S1.b) which promotes both fast and slow flow towards eastern direction.

612 **5.2 Understanding physical controls and spatial variation of seasonal flow duration curve using mid-section** 613 **slope**

614 Apart from mean, variance and no-flow frequency, the midsection slope of the FDC – estimated using
615 $\frac{\ln(Q_{33p}) - \ln(Q_{66p})}{0.66 - 0.33}$, where Q_{33p} and Q_{66p} represent the streamflow values at 33rd and 66th percentiles respectively –
616 is connected to the average flow regime of the catchment, which is controlled by both surface and subsurface
617 processes (Yokoo & Sivapalan, 2011; Chouaib et al., 2018). The association of the slope of FDC with the
618 parameters pertaining to recession analysis is presented in Fig. 13.



621 **Figure 13.** Association between streamflow variability and recession parameters.

622 During Non-monsoon and North East monsoon seasons (Fig. 13a and Fig. 13c) – when rainfall is comparatively
623 less than South West monsoon – a significant association between flow variability and β highlights the importance
624 of slow flow and recession characteristics controlled by aquifer geometry and water table elevation profile. In
625 addition to significant association with β during South West monsoon (Fig. 13b), the midsection slope of FDC is
626 positively correlated with γ – the parameter which is strongly related with the seasonality of catchment wetness,
627 evapotranspiration and spatial variation in rainfall – revealing the importance of land surface processes in
628 variability of streamflow variability.

629 A coherent pattern in variability of streamflow (via. Midsection slope of FDC) is observed across South – North
630 gradient of the Peninsular region (Fig. 13e). This systematic pattern in streamflow variability reflects the influence
631 of combined functioning of subsurface and land surface processes on regional hydrologic signatures of Peninsular
632 India.

633 **6. Conclusions**

634 The comprehensive analysis of spatial variations in seasonal and annual flow duration curves across Peninsular
635 India has provided valuable insights into the controls of streamflow variability at different scales. The partitioning
636 framework employed in this study effectively approximated annual flow duration curves, confirming its efficacy
637 in capturing the intricate dynamics of seasonal and monthly flows. Noteworthy spatial patterns emerged, with
638 gauging stations in the northern part of the peninsula exhibiting higher dominance of South-West monsoon flows
639 in contrast to the more balanced contributions observed in the southern regions, where North-East monsoon flows
640 also played a significant role.

641 The regional-scale analysis unveiled the influence of spatial patterns of monsoon rainfall, showing increased
642 contributions of South-West monsoon flows in the northerly direction and elevated contributions of North-East
643 monsoon flows in the southerly direction. The study also delved into the partitioning of streamflow into fast and
644 slow components, revealing a dominance of fast flow in northern basins and an increasing contribution of slow
645 flow in the southerly direction. Factors such as rainfall intensity, geologic formations, and groundwater gradients
646 were identified as critical controls shaping these flow characteristics. The investigation of combined influences
647 of climatic time scales and process time scales further enriched our understanding of streamflow variability.
648 Seasonal fluctuations in fast and slow flow contributions highlighted the dynamic nature of streamflow response
649 to monsoon onset and withdrawal. The study emphasized the importance of considering both climatic and
650 landscape factors across different scales to comprehensively grasp the controls of streamflow variability in the
651 Peninsular region.

652 By undertaking an extensive analysis of flow duration curves for both fast and slow flow components across
653 different seasons, the study aims to understand the variations and controls governing these hydrological patterns.
654 The initial step of scaling the fast and slow flow time series by their respective long-term mean values serves as
655 a crucial tool in isolating secondary controls on FDC shapes, effectively removing the influence of mean climate
656 and geology. The subsequent use of the Mixed Gamma Distribution to fit the scaled time series allows for an
657 advanced examination of the parameters influencing FDC shapes, with a focus on the key factors of shape
658 parameter (k) and probability of zero flows (α). The seasonal variations of MGD parameters at a regional scale

659 reveal the impact of monsoons on streamflow characteristics. Notably, the consistently higher shape parameters
660 for slow flow highlight the lower variance attributed to longer residence times in subsurface formations,
661 emphasizing the influence of geological features.

662 Further exploration into the relationships between MGD parameters and landscape properties through recession
663 analysis enhances our understanding of hydrological controls. The positive correlation between the shape
664 parameter of slow flow and recession parameter β , influenced by aquifer geometry, contrasts with the negative
665 correlation between the shape parameter of fast flow and the parameter γ , associated with seasonality of catchment
666 wetness and evapotranspiration. Spatial variation analysis using descriptors like latitude, longitude, and catchment
667 area unveils significant correlations, offering insights into the influence of geographical factors on FDC shapes.
668 The correlation of fast flow shape parameters with catchment area suggests reduced variability in larger
669 catchments, while the negative correlation of slow flow shape parameters with latitude indicates increased
670 variability in the northern part of the region. The examination of zero-flow probabilities controlled by the
671 parameter α reveals noteworthy trends. Larger catchments exhibit lower zero-flow probabilities, and the negative
672 correlation of α with longitude highlights the spatial influence along the west-east direction. Finally, the study
673 explores the midsection slope of the FDC, connecting it to average flow regimes controlled by both surface and
674 subsurface processes. Associations with recession analysis parameters underline the integrated influence of
675 aquifer geometry and land surface processes on streamflow variability across Peninsular India.

676 In summary, the methodology employed in this study offers a systematic and insightful approach to unravelling
677 the complexities of streamflow variability across Peninsular India. This study not only enhances our understanding
678 of the relative contributions and shapes of FDCs but also sheds light on the intricate interplay of geological,
679 spatial, and hydrological factors influencing streamflow variability in this region.

680 We acknowledge, however, that in recent times streamflow variability in Peninsular India has been significantly
681 impacted by anthropogenic activities, including significant land use and land cover changes, and other human
682 interferences such as the building of dams and the extraction of water from both rivers and from groundwater
683 aquifers for human use. The present study has not explored the effects of human impacts: their impacts on both
684 temporal (inter-decadal) and spatial (regional) variations of the FDCs is left for future work. Further work is also
685 needed to understand in more detail the causes and the relative contributions of regional patterns precipitation and
686 geological formations on streamflow partitioning.

687 On the methodological front, there is opportunity to refine the analysis used here to incorporate the statistical
688 cross-correlation between fast and slow flows in the reconstruction of the FDC for total streamflow, by adopting
689 generalized approaches (e.g., copulas). In the exploration of the relative contributions of the monsoons, there is
690 scope to extend the analysis framework to partition the streamflow variability guided by the actual breakdown
691 into the seasons each year in a more flexible way, as opposed to the static way. This is likely to make the results
692 of the analysis more robust and less uncertain. Finally, in the process domain, the filter-based separation of total
693 streamflow into fast and slow flow can be variably impacted by catchment size, introducing some uncertainty into
694 the partitioning of the FDC of total streamflow into its fast flow and slow flow components. Future work in this
695 area should explore ways to overcome these methodological shortcomings.

696

697 *Data availability.* The streamflow datasets used for the analysis are accessible from
698 <https://indiawris.gov.in/wris/#/>. The daily India Meteorological Department (IMD) gridded rainfall product at
699 spatial resolution of $0.25^\circ \times 0.25^\circ$
700 (https://www.imdpune.gov.in/Clim_Pred_LRF_New/Grided_Data_Download.html) from Pai et al., (2014) is
701 used. The function baseflow, used for partitioning total flow to slow flow is downloaded from
702 [https://in.mathworks.com/matlabcentral/fileexchange/58525-baseflow-filter-using-the-recursive-digital-filter-](https://in.mathworks.com/matlabcentral/fileexchange/58525-baseflow-filter-using-the-recursive-digital-filter-technique)
703 [technique](https://in.mathworks.com/matlabcentral/fileexchange/58525-baseflow-filter-using-the-recursive-digital-filter-technique).

704 *Author contributions.* PD, JM, and MS conceptualized the work, developed the methodology, and carried out the
705 data curation, formal analysis, validation, and writing of the original draft. MS and PPM reviewed the initial
706 manuscript, and PPM provided the resources needed for this work.

707 *Competing interests.* The authors declare that they have no conflict of interest.

708 *Acknowledgements.* PD acknowledges DST INSPIRE Faculty Fellowship (DST/INSPIRE/04/2022/001952
709 Faculty Reference No.: IFA22-EAS 114) received from Department of Science and Technology, Government of
710 India, in Earth and Atmospheric Sciences Division of 2022 call. MS acknowledges the award of a Satish Dhawan
711 Endowed Visiting Professorship that enabled him to visit the Interdisciplinary Centre for Water Research
712 (ICWaR) at the Indian Institute of Science, which allowed him to participate in the research activity that
713 culminated in this paper. MS also acknowledges the generous support and facilities provided by ICWaR that made
714 his stay a very productive one.

715

716 **References**

717 Arai, R., Toyoda, Y., & Kazama, S. (2021). Runoff recession features in an analytical probabilistic streamflow
718 model. *Journal of Hydrology*, 597, 125745.

719 Arulbalaji, P., Sreelash, K., Maya, K., and Padmalal, D.: Hydrological assessment of groundwater potential zones
720 of Cauvery River Basin, India: a geospatial approach, *Environ. Earth Sci.*, 78, 1–21,
721 <https://doi.org/10.1007/s12665-019-8673-6>, 2019.

722 Basso, S. and Botter, G.: Streamflow variability and optimal capacity of run-of-river hydropower plants, *Water*
723 *Resour. Res.*, 48, 1–13, <https://doi.org/10.1029/2012WR012017>, 2012.

724 Basso, S., Schirmer, M., & Botter, G. (2015). On the emergence of heavy-tailed streamflow distributions.
725 *Advances in Water Resources*, 82, 98-105.

726 Biswal, B. and Nagesh Kumar, D.: Study of dynamic behaviour of recession curves, *Hydrol. Process.*, 28, 784–
727 792, <https://doi.org/10.1002/hyp.9604>, 2014.

728 Blum, A. G., Archfield, S. A., Vogel, R. M., and Survey, G.: On the probability distribution of daily streamflow
729 in the United States, *Hydrol. Earth Syst. Sci.*, 21, 3093–3103, [https://doi.org/https://doi.org/10.5194/hess-21-](https://doi.org/https://doi.org/10.5194/hess-21-3093-2017)
730 [3093-2017](https://doi.org/https://doi.org/10.5194/hess-21-3093-2017), 2017.

731 Botter, G., Zanardo, S., Porporato, A., Rodriguez-Iturbe, I., and Rinaldo, A.: Ecohydrological model of flow
732 duration curves and annual minima, *Water Resour. Res.*, 44, 1–12, <https://doi.org/10.1029/2008WR006814>, 2008.

733 Botter, G., Basso, S., Rodriguez-Iturbe, I., & Rinaldo, A. (2013). Resilience of river flow regimes. *Proceedings*
734 *of the National Academy of Sciences*, 110(32), 12925-12930.

735 Carlier, C., Wirth, S. B., Cochand, F., Hunkeler, D., & Brunner, P. (2018). Geology controls streamflow dynamics.
736 *Journal of Hydrology*, 566, 756-769.

737 Chandra, P. C.: Groundwater of Hard Rock Aquifers of India, 61–84, [https://doi.org/10.1007/978-981-10-3889-](https://doi.org/10.1007/978-981-10-3889-1_5)
738 [1_5](https://doi.org/10.1007/978-981-10-3889-1_5), 2018.

739 Chatterjee, S., Scotese, C. R., and Bajpai, S.: The Restless Indian plate and its epic voyage from Gondwana to
740 Asia: Its tectonic, paleoclimatic, and paleobiogeographic evolution, *Spec. Pap. Geol. Soc. Am.*, 529, 1–147,
741 <https://doi.org/10.1130/2017.2529>, 2017.

742 Cheng, L., Yaeger, M., Viglione, A., Coopersmith, E., Ye, S., and Sivapalan, M.: Exploring the physical controls

- 743 of regional patterns of flow duration curves – Part 1: Insights from statistical analyses, *Hydrol. Earth Syst.*
744 *Sci.*, 16, 4435–4446, <https://doi.org/10.5194/hess-16-4435-2012>, 2012.
- 745 Chouaib, W., Caldwell, P. V., and Alila, Y.: Regional variation of flow duration curves in the eastern United
746 States: Process-based analyses of the interaction between climate and landscape properties, *J. Hydrol.*, 559, 327–
747 346, <https://doi.org/10.1016/j.jhydrol.2018.01.037>, 2018.
- 748 Collins, L. S., Loveless, S. E., Muddu, S., Buvaneshwari, S., Palamakumbura, R. N., Krabbendam, M., Lapworth,
749 D. J., Jackson, C. R., Gooddy, D. C., Nara, S. N. V., Chattopadhyay, S., and MacDonald, A. M.: Groundwater
750 connectivity of a sheared gneiss aquifer in the Cauvery River basin, India, *Hydrogeol. J.*, 28, 1371–1388,
751 <https://doi.org/10.1007/s10040-020-02140-y>, 2020.
- 752 Costa, V. and Fernandes, W.: Regional Modeling of Long-Term and Annual Flow Duration Curves: Reliability
753 for Information Transfer with Evolutionary Polynomial Regression, *J. Hydrol. Eng.*, 26, 1–12,
754 [https://doi.org/10.1061/\(asce\)he.1943-5584.0002051](https://doi.org/10.1061/(asce)he.1943-5584.0002051), 2021.
- 755 Das, S.: Frontiers of Hard Rock Hydrogeology in India, in: *Ground Water Development - Issues and Sustainable*
756 *Solutions*, Springer Singapore, Singapore, 35–68, https://doi.org/10.1007/978-981-13-1771-2_3, 2019.
- 757 Deshpande, N. R., Kothawale, D. R., and Kulkarni, A.: Changes in climate extremes over major river basins of
758 India, *Int. J. Climatol.*, 36, 4548–4559, <https://doi.org/10.1002/joc.4651>, 2016.
- 759 Dralle, D., Karst, N., and Thompson, S. E.: a, b careful: The challenge of scale invariance for comparative analyses
760 in power law models of the streamflow recession, *Geophys. Res. Lett.*, 42, 9285–9293,
761 <https://doi.org/10.1002/2015GL066007>, 2015.
- 762 Durigetto, N., Mariotto, V., Zanetti, F., McGuire, K. J., Mendicino, G., Senatore, A., & Botter, G. (2022).
763 Probabilistic description of streamflow and active length regimes in rivers. *Water Resources Research*, 58,
764 e2021WR031344. <https://doi.org/10.1029/2021WR031344>
- 765 Gadgil, S.: The Indian Monsoon and Its Variability, *Annu. Rev. Earth Planet. Sci.*, 31, 429–467,
766 <https://doi.org/10.1146/annurev.earth.31.100901.141251>, 2003.
- 767 Fenicia, F., Kavetski, D., Savenije, H. H., Clark, M. P., Schoups, G., Pfister, L., & Freer, J. (2014). Catchment
768 properties, function, and conceptual model representation: is there a correspondence? *Hydrological Processes*,
769 28(4), 2451–2467.
- 770 Ghotbi, S., Wang, D., Singh, A., Blöschl, G., and Sivapalan, M.: A New Framework for Exploring Process
771 Controls of Flow Duration Curves, *Water Resour. Res.*, 56, <https://doi.org/10.1029/2019WR026083>, 2020a.
- 772 Ghotbi, S., Wang, D., Singh, A., Mayo, T., and Sivapalan, M.: Climate and Landscape Controls of Regional
773 Patterns of Flow Duration Curves Across the Continental United States: Statistical Approach, *Water Resour. Res.*,
774 56, <https://doi.org/10.1029/2020WR028041>, 2020b.
- 775 Gnann, S. J., McMillan, H. K., Woods, R. A., and Howden, N. J. K.: Including Regional Knowledge Improves
776 Baseflow Signature Predictions in Large Sample Hydrology, *Water Resour. Res.*, 57,
777 <https://doi.org/10.1029/2020WR028354>, 2021.
- 778 Harini, P., Sahadevan, D. K., Das, I. C., Manikyamba, C., Durgaprasad, M., and Nandan, M. J.: Regional
779 Groundwater Assessment of Krishna River Basin Using Integrated GIS Approach, *J. Indian Soc. Remote Sens.*,
780 46, 1365–1377, <https://doi.org/10.1007/s12524-018-0780-4>, 2018.
- 781 Harman, C. and Troch, P. A.: What makes Darwinian hydrology “Darwinian”? Asking a different kind of question
782 about landscapes, *Hydrol. Earth Syst. Sci.*, 18, 417–433, <https://doi.org/10.5194/hess-18-417-2014>, 2014.
- 783 Kale, V. S., Hire, P., and Baker, V. R.: Flood Hydrology and Geomorphology of Monsoon-dominated Rivers:
784 The Indian Peninsula, *Water Int.*, 22, 259–265, <https://doi.org/10.1080/02508069708686717>, 1997.
- 785 Kale, V. S., Vaidyanadhan, R.: *Landscapes and Landforms of India*, edited by: Kale, V. S., Springer Netherlands,
786 Dordrecht, 105–113 pp., https://doi.org/10.1007/978-94-017-8029-2_6, 2014.
- 787 Krishnamurthy, V. and Ajayamohan, R. S.: Composite Structure of Monsoon Low Pressure Systems and Its
788 Relation to Indian Rainfall, *J. Clim.*, 23, 4285–4305, <https://doi.org/10.1175/2010JCLI2953.1>, 2010.
- 789 Krasovskaia, I., Gottschalk, L., Leblois, E., & Pacheco, A. (2006). Regionalization of flow duration curves.
790 *Climate variability and change: hydrological impacts*, 105–110.

791 Leong, C., & Yokoo, Y. (2019). An interpretation of the relationship between dominant rainfall-runoff processes
792 and the shape of flow duration curve by using data-based modeling approach. *Hydrological Research Letters*,
793 13(4), 62-68.

794 Leong, C., & Yokoo, Y. (2022). A multiple hydrograph separation technique for identifying
795 hydrological model structures and an interpretation of dominant process controls on flow
796 duration curves. *Hydrological Processes*, 36(4), e14569. <https://doi.org/10.1002/hyp.14569>

797 Magilligan, F. J. and Nislow, K. H.: Changes in hydrologic regime by dams, *Geomorphology*, 71, 61–78,
798 <https://doi.org/10.1016/j.geomorph.2004.08.017>, 2005.

799 Magilligan, F. J., Nislow, K. H., and Graber, B. E.: Scale-independent assessment of discharge reduction and
800 riparian disconnectivity following flow regulation by dams, *Geology*, 31, 569, [https://doi.org/10.1130/0091-7613\(2003\)031<0569:SAODRA>2.0.CO;2](https://doi.org/10.1130/0091-7613(2003)031<0569:SAODRA>2.0.CO;2), 2003.

802 Müller, M. F., & Thompson, S. E. (2016). Comparing statistical and process-based flow duration curve models in
803 ungauged basins and changing rain regimes. *Hydrology and Earth System Sciences*, 20(2), 669-683.

804 Narasimhan, T. N.: Ground Water in Hard-Rock Areas of Peninsular India: Challenges of Utilization, *Ground*
805 *Water*, 44, 130–133, <https://doi.org/10.1111/j.1745-6584.2005.00167.x>, 2006.

806 Pai, D. S., Sridhar, L., Rajeevan, M., Sreejith, O. P., Satbhai, N. S., and Mukhopadhyay, B.: Development of a
807 new high spatial resolution (0.25° × 0.25°) long period (1901-2010) daily gridded rainfall data set over India and
808 its comparison with existing data sets over the region, *Mausam*, 1, 1–18, 2014.

809 Patil, S., Kulkarni, H., Bhave, N., Development, W. R., Forum, P., Dialogue, P., and Conflicts, W.: Groundwater
810 in the Mahanadi River Basin, <https://doi.org/10.13140/RG.2.2.11561.95846>, 2017.

811 Prakash, S., Mitra, A. K., and Pai, D. S.: Comparing two high-resolution gauge-adjusted multisatellite rainfall
812 products over India for the southwest monsoon period, *Meteorol. Appl.*, 22, 679–688,
813 <https://doi.org/10.1002/met.1502>, 2015.

814 Rajeevan, M., Unnikrishnan, C. K., Bhate, J., Niranjana Kumar, K., and Sreekala, P. P.: Northeast monsoon over
815 India: variability and prediction, *Meteorol. Appl.*, 19, 226–236, <https://doi.org/10.1002/met.1322>, 2012.

816 Ramachandra, T. V: Global Biodiversity Hotspot - Western Ghats : Water Tower of Peninsular India and Precious
817 Heritage for Posterity, 2018.

818 Rehana, S. and Mujumdar, P. P.: River water quality response under hypothetical climate change scenarios in
819 Tunga-Bhadra river, India, *Hydrol. Process.*, 25, 3373–3386, <https://doi.org/10.1002/hyp.8057>, 2011.

820 Rehana, S. and Mujumdar, P. P.: Climate change induced risk in water quality control problems, *J. Hydrol.*, 444–
821 445, 63–77, <https://doi.org/10.1016/j.jhydrol.2012.03.042>, 2012.

822 Richards, F. D., Hoggard, M. J., and White, N. J.: Cenozoic epeirogeny of the Indian peninsula, *Geochemistry*,
823 *Geophys. Geosystems*, 17, 4920–4954, <https://doi.org/10.1002/2016GC006545>, 2016.

824 Saha, K. R., Mooley, D. A., and Saha, S.: The Indian monsoon and its economic impact, *GeoJournal*, 3,
825 <https://doi.org/10.1007/BF00257706>, 1979.

826 Santos, A. C., Portela, M. M., Rinaldo, A., & Schaeffli, B. (2018). Analytical flow duration curves for summer
827 streamflow in Switzerland. *Hydrology and earth system sciences*, 22(4), 2377-2389.

828 Searcy, J. K.: Flowduration curves, *Man. Hydrol. U.S. Geol. Surv.*, 1959.

829 Sinha, J., Sharma, A., Khan, M., and Goyal, M. K.: Assessment of the impacts of climatic variability and
830 anthropogenic stress on hydrologic resilience to warming shifts in Peninsular India, *Sci. Rep.*, 8, 13833,
831 <https://doi.org/10.1038/s41598-018-32091-0>, 2018.

832 Sivapalan, M.: From engineering hydrology to Earth system science: milestones in the transformation of
833 hydrologic science, *Hydrol. Earth Syst. Sci.*, 22, 1665–1693, <https://doi.org/10.5194/hess-22-1665-2018>, 2018.

834 Smakhtin, V. U.: Smakhtin 2010- Low flow hydrology.pdf, *J. Hydrol. Hydrol.*, 240, 147–186,
835 [https://doi.org/10.1016/S0022-1694\(00\)00340-1](https://doi.org/10.1016/S0022-1694(00)00340-1), 2001.

- 836 Stewart, M. K. (2015). Promising new baseflow separation and recession analysis methods
837 applied to streamflow at Glendhu Catchment, New Zealand. *Hydrology and Earth System*
838 *Sciences*, 19(6), 2587-2603.
- 839 Tashie, A., Pavelsky, T., and Band, L. E.: An Empirical Reevaluation of Streamflow Recession Analysis at the
840 Continental Scale, *Water Resour. Res.*, 56, <https://doi.org/10.1029/2019WR025448>, 2020a.
- 841 Tashie, A., Pavelsky, T., and Emanuel, R. E.: Spatial and Temporal Patterns in Baseflow Recession in the
842 Continental United States, *Water Resour. Res.*, 56, <https://doi.org/10.1029/2019WR026425>, 2020b.
- 843 Tongal, H., Demirel, M. C., and Moradkhani, H.: Analysis of dam-induced cyclic patterns on river flow dynamics,
844 *Hydrol. Sci. J.*, 62, 626–641, <https://doi.org/10.1080/02626667.2016.1252841>, 2017.
- 845 Vogel, R. M. and Fennessey, N. M.: Flow-Duration Curves. I: New Interpretation and Confidence Intervals, *J.*
846 *Water Resour. Plan. Manag.*, 120, 485–504, [https://doi.org/10.1061/\(ASCE\)0733-9496\(1994\)120:4\(485\)](https://doi.org/10.1061/(ASCE)0733-9496(1994)120:4(485)), 1994.
- 847 Vogel, R. M. and Fennessey, N. M.: Flow Duration Curves Ii: a Review of Applications in Water Resources
848 Planning, *JAWRA J. Am. Water Resour. Assoc.*, 31, 1029–1039, [https://doi.org/10.1111/j.1752-](https://doi.org/10.1111/j.1752-1688.1995.tb03419.x)
849 [1688.1995.tb03419.x](https://doi.org/10.1111/j.1752-1688.1995.tb03419.x), 1995.
- 850 Wagener, T., Blöschl, G., Goodrich, D. C., Gupta, H. V., Sivapalan, M., Tachikawa, Y., Troch, P. A., and Weiler,
851 M.: A synthesis framework for runoff prediction in ungauged basins, in: *Runoff Prediction in Ungauged Basins*,
852 Cambridge University Press, 11–28, <https://doi.org/10.1017/CBO9781139235761.005>, 2013.
- 853 Ye, S., Yaeger, M., Coopersmith, E., Cheng, L., & Sivapalan, M. (2012). Exploring the physical controls of
854 regional patterns of flow duration curves–Part 2: Role of seasonality, the regime curve, and associated process
855 controls. *Hydrology and Earth System Sciences*, 16(11), 4447-4465.
- 856 Yokoo, Y. and Sivapalan, M.: Towards reconstruction of the flow duration curve: Development of a conceptual
857 framework with a physical basis, *Hydrol. Earth Syst. Sci.*, 15, 2805–2819, [https://doi.org/10.5194/hess-15-2805-](https://doi.org/10.5194/hess-15-2805-2011)
858 [2011](https://doi.org/10.5194/hess-15-2805-2011), 2011.
- 859